Feasibility of a Nuclear Recoil Observatory with Directional Sensitivity to WIMPs and Solar Neutrinos

A. Author[1]

Abstract

Now that conventional WIMP dark matter searches are approaching the neutrino floor, there has been a resurgence of interest in the possibility of introducing recoil direction sensitivity into the field. Such directional sensitivity would offer the powerful prospect of reaching below this floor, introducing both the possibility of identifying a clear signature for dark matter particles in the galaxy below this level but also of exploiting observation of coherent neutrino scattering from the Sun and other sources with directional sensitivity. We survey the experimental status of all technologies proposed to date, and perform a cost-benefit analysis to identify the optimal choice in different WIMP and neutrino scenarios. Based on our findings, we propose a large-scale directional nuclear recoil observatory with directional WIMP sensitivity below the neutrino floor and capability to explore Solar neutrino coherent scattering with direction sensitivity

Keywords: keyword1, keyword2

Contents

1. Introduction

[Section organizer: all]

The aim of this paper is to lay out the science case and goals for a large galactic recoil observatory, to show that the goals are achievable in principle, to compare the capability of different technologies to reach those goals. Here is a citation [1].

2. Science Case for a large Nuclear Recoil Observatory

[Section organizer: Katie Mack]

2.1. *Dark matter*

[KM, COH]

The primary method of directly detecting WIMP dark matter is by the observation of nuclear recoils with energies of $O(1-100)$ keV. Experiments have been carried out using a wide range of targets, with recoil detection via charge, light, or heat (phonon) signals (for a review see e.g. Ref. [2]). Direct detection experiments have constrained WIMP masses and nucleon cross sections, with the tightest limits challenging favored supersymmetric WIMP models. Several experiments have also reported detections that are consistent with a dark matter interpretation but are inconsistent with stringent limits made by other experiments. One notable example is the DAMA/LIBRA collaboration which has reported a 9.3σ annual modulating event rate in their NaI crystal scintillator [3]. The phase and amplitude of this modulation is consistent with expectation for a signal of Galactic origin, due to the unique orientation of the Earth's orbit with respect to orbit of the Sun around the Milky Way center. Efforts are being made to reproduce this experiment in the Southern Hemisphere with alternative crystals to rule out target-specific effects and to eliminate seasonal variations as an explanation for the modulation [4, 5, 6].

Meanwhile, *directional* detection experiments present a new opportunity for discovery in this space. With directional capability, detectors have a strongly enhanced ability to remove backgrounds. In addition to the annually modulating signal, the orbit of the Solar System through the non-rotating Milky Way halo means the dark matter flux observed at Earth should also be strongly anisotropic. This "WIMP wind" should peak towards the direction of the constellation Cygnus [7]. This property would be observable in a directional experiment, but not otherwise. Hence the measurement of the directions of nuclear recoils is the only way to make an unequivocal claim that the source of some excess in events is the same particle that makes up the dark matter in the Milky Way. Hence in the ideal case, directional capability will make a potential WIMP search maximally reliable and robust through (1) confirmation of the connection between signal events and the Galactic halo, i.e. the discovery of dark matter [8]; (2) elimination of neutrino backgrounds that are irreducible without directional sensitivity [9, 10]. Furthermore a directional experiment would much better suited to study the astrophysical velocity structure of the dark matter halo [11] and improve the detection of, or constraints on, particular WIMP particle physics models with directional dependent features. We describe each of these points in Secs. 2.1.1-2.1.4.

Ongoing directional detection experiments such as DRIFT [12], MIMAC [13], DMTPC [14] and NEWAGE [15] have demonstrated a proof of concept, but would require vast up-scaling to compete with the most stringent limits. Our proposed detection method will provide the opportunity to strongly improve directional limits and to discover Galactic dark matter.

2.1.1. *WIMP scattering review*

The event rate for WIMP induced nuclear recoils is derived by integrating the incoming flux of dark matter with the cross section, σ, for the WIMP-nucleus interaction. This is usually written in terms of the differential event rate R per unit detector mass, as a function of recoil energy E and time t,

$$\frac{\mathrm{d}R}{\mathrm{d}E}(E,t) = \frac{\rho_0}{m_\chi m_A} \int_{v>v_{\rm min}} v f(\mathbf{v},t) \frac{\mathrm{d}\sigma}{\mathrm{d}E}(E,v) \mathrm{d}^3 v \quad (1)$$

where ρ_0 is the local dark matter mass density, m_χ is the WIMP mass, m_A is the nucleus mass, $\mathbf{v}$ is the dark matter velocity in the detector rest frame. The integral is performed for speeds larger than $v_{\rm min}(E) = \sqrt{m_A E/2\mu_{\chi A}}$ which is the minimum speed capable of inducing a recoil with energy E. The integral is weighted by the velocity distribution, $f(\mathbf{v},t)$ which is usually assumed to be constant in the Galactic frame, but picks up a time dependence after a boost into the laboratory rest frame. The differential cross section is proportional to the squared matrix element for a particular WIMP-nucleus interaction, so is therefore specifically

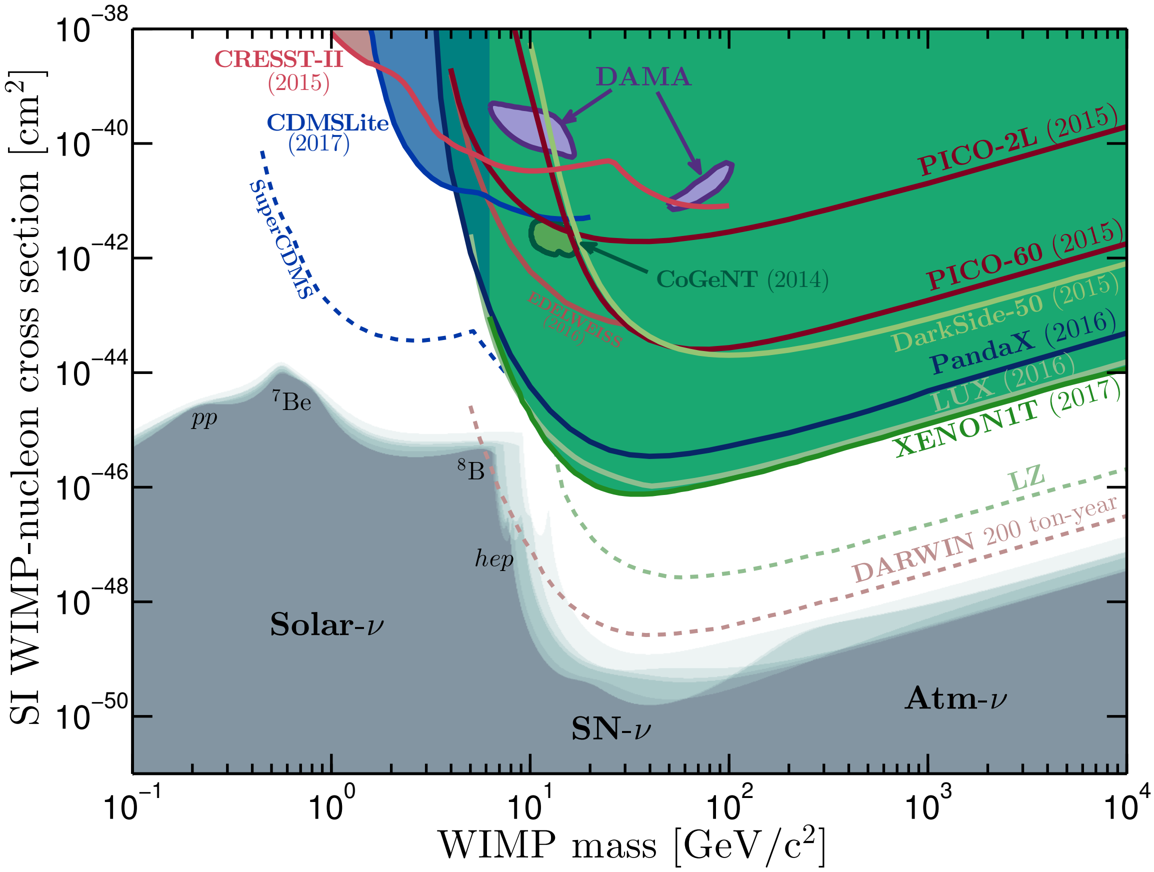

Figure 1: Existing and projected constraints on the spin-independent WIMP-nucleon cross section as a function of WIMP mass. Constraints and detection regions for different experiments are labelled in the plot. The existing constraints as of 2017 are, CRESST-II [16], CDMSLite [17], EDELWEISS-III [18], PICO-2L [19], PICO-60 [20], DarkSide-50 [21], PandaX [22], LUX [23], XENON1T [24]. The projected limits are estimated for the SuperCDMS [25], LZ [26] and DARWIN [27] experiments. The closed detection regions correspond to the DAMA/LIBRA [3] and CoGeNT [28] annual modulation signals. Below the existing limits we dispay the neutrino floor for various target nuclei as shaded grey regions. The neutrino background responsible for the floor is displayed (from low to high mass): Solar neutrinos, the diffuse supernova neutrino background and atmospheric neutrinos. We discuss the neutrino floor in Sec. 2.1.2.

model dependent. However one can work with general formulae. The most common approach is to divide the interaction into two possible channels, both of which may contribute to the total rate,

$$\frac{d\sigma}{dE} = \frac{m_A}{2\mu_{\chi A}^2 v^2}\left(\sigma_0^{\rm SI} F_{\rm SI}^2(E) + \sigma_0^{\rm SD} F_{\rm SD}^2(E)\right) . \tag{2}$$

Here, the first term describes spin-independent (SI) interactions such as those arising from scalar or vector WIMP-quark couplings, whereas the second includes the spin-dependent (SD) from axial-vector couplings. The factor $\mu_{\chi A}$ is the WIMP-nucleus reduced mass. The cross sections $\sigma_0^{\rm SI,SD}$ are defined at zero momentum transfer, so that the form factors $F_{\rm SI,SD}^2$ are used to describe how the spatial extent of the nucleus causes a loss in coherence in the interaction towards larger momentum transfers. Note that the form factors are entirely nuclear physics dependent and all WIMP particle physics is contained in the values of $\sigma_0^{\rm SI\,SD}$.

Constraints on SI and SD cross sections vary, as they employ different assumptions about the interactions between the WIMP and the nucleon. In the SI case the total nuclear cross section is enhanced by the number of nucleons squared, meaning that large target nuclei can be used to set very stringent limits. In the spin-dependent case, the interaction probability is not amplified, and depends on the spin content of the target nuclei, hence constraints tend to be weaker. Figure 1 shows a selection of constraints from direct detection experiments. Constraints exist for WIMPs with masses larger than ∼ 1 GeV and SI cross sections larger than $\sim 10^{-46}$ cm^2. Underneath these limits lies the neutrino floor, below which WIMP models are rendered unobservable due to the saturation of their signal by the irreducible background from coherent neutrino-nucleus scattering (to be discussed in Sec. 2.1.2).

In the case of directional detectors the relevant differential event rate is modified to be a function of both recoil energy and direction. The formula for this event rate is derived by enforcing the kinematical relationship between the incoming WIMP velocity, $\mathbf{v}$, with the outgoing recoil direction $\hat{\mathbf{r}}$ [29],

$$\frac{\mathrm{d}^2\sigma}{\mathrm{d}E\,\mathrm{d}\Omega} = \frac{\mathrm{d}\sigma}{\mathrm{d}E}\frac{1}{2\pi} v\,\delta\left(\mathbf{v}\cdot\hat{\mathbf{r}} - v_{\rm min}\right)\,, \tag{3}$$

where $\mathrm{d}\Omega$ is the solid angle element around $\hat{\mathbf{r}}$. The event rate then has the structure,

$$\frac{\mathrm{d}^2 R}{\mathrm{d}E\mathrm{d}\,\Omega}(E,\hat{\mathbf{r}},t) = \frac{\rho_0}{4\pi\mu^2_{\chi p} m_\chi}(\sigma_0^{\rm SI} F^2_{\rm SI}(E) + \sigma_0^{\rm SD} F^2_{\rm SD}(E))\,\hat{f}(v_{\rm min},\hat{\mathbf{r}},t)\,. \tag{4}$$

where the velocity distribution now enters in the form of its Radon transform,

$$\hat{f}(v_{\rm min},\hat{\mathbf{r}},t) = \int \delta\left(\mathbf{v}\cdot\hat{\mathbf{r}} - v_{\rm min}\right) f(\mathbf{v},t)\,\mathrm{d}^3\mathbf{v}\,. \tag{5}$$

The unique anisotropic character of the radon transform of the local dark matter velocity distribution when observed in the detector rest frame is the reason why directional detection is such a powerful method of detecting dark matter. The primary signal is a dipole anisotropy towards the direction $\hat{\mathbf{r}} = -\hat{\mathbf{v}}_{\rm lab}$ where $\mathbf{v}_{\rm lab}$ is the velocity of the laboratory. As first calculated in Ref. [7] this would result in an $\mathcal{O}(10)$ forward-backward asymmetry in the number of events. The prominence of the dipole feature means that in ideal circumstances (i.e. perfect recoil direction reconstruction) an isotropic assumption for the recoil direction distribution can be rejected at 90% confidence with only $\mathcal{O}(10)$ events, with no recoil energy information needed [30]. With $\mathcal{O}(30)$ recoil directions it becomes possible to point back towards Cygnus and confirm the Galactic origin of the signal [31]. Secondary signals such as a ring feature at low energies [32], and the aberration of recoil directions over time [33], may also aid in the confirmation of a dark matter signal.

2.1.2. WIMP detection below the neutrino floor

[COH]

It was anticipated in early work on direct dark matter detection that large detectors would eventually become sensitive to coherent scattering between neutrinos and nuclei [34]. For the keV nuclear recoil energy scales observed in direct detection experiments Solar, diffuse supernovae and atmospheric neutrinos all constitute a significant background for detector exposures beyond the ton-year scale [35, 36, 37]. Because neutrinos are impossible to shield they represent the ultimate background for the direct detection of WIMPs. Moreover, because the nuclear recoil energy spectra induced by coherent neutrino-nucleus scattering mimics the spectra for WIMPs of certain masses, the discovery of these characteristic masses is limited due to the sizable systematic uncertainty on the expected neutrino flux. The range of cross sections that are reached by an experiment that has sufficient sensitivity to be also subject to a dominating neutrino background is known as the "neutrino floor" [38]. The shape of the neutrino floor is dependent on the flux of each neutrino background component as well as, importantly, the uncertainty on this flux. The most notable and threatening feature in the neutrino floor is the shoulder just below WIMP masses of $\sim$10 GeV due to the large flux and low energies of Solar neutrinos. The most important of these are the neutrinos originating from ^{8}B decay. In a xenon experiment the nuclear recoil signal due to a 6 GeV WIMP with a SI cross section around 5×10^{-45} cm^2 is well matched by ^{8}B neutrinos. Towards slightly larger masses (10 - 30 GeV) the neutrino floor is set by the diffuse supernova neutrino background (DSNB) due to the cumulative emission of neutrinos from a cosmological history of supernovae. The expected flux of the DSNB is extremely low ($\sim$ 80 cm^2 s^{-1} [39]) so the neutrino floor at these intermediate masses falls by several orders of magnitude in cross section. Towards masses beyond 100 GeV the neutrino floor is induced by the low energy tail of atmospheric neutrinos from cosmic ray interactions in the upper atmosphere. Atmospheric neutrinos are the only significant background contributing neutrino energies above 100 MeV. The low energy tail of atmospheric neutrinos is difficult to both measure and theoretically predict [40] so currently has uncertainties of around 20% [41].

A central challenge for the next generation of dark matter experiment is how to continue the search for dark matter WIMPs to cross sections below the neutrino floor. However, it is important to emphasise that despite the nomenclature, the neutrino floor is not a hard limit to direct detection. This is because the neutrino background is not strictly irreducible, even in conventional experiments. While the nuclear recoil energies of coherent neutrino-nucleus scattering and WIMP-nucleus scattering are very similar, the spectra do not exhibit perfect matching, even for masses best mimicked by neutrinos. As initially shown by Ruppin *et al* [42], the neutrino background can be subtracted with recoil energy information alone for very high statistics due to the slight differences in the tails of the recoil energy distributions. Unfortunately this requires prohibitively large experimental exposures, usually in excess of 1000 ton-years. It has also been shown that for some of the additional operators posited in the non-relativistic effective field theory formalism, the recoil spectra are sufficiently distinct from neutrinos to allow their discrimination with fewer events than in the standard SI or SD cases [43, 44]. However the overlap between the WIMP signal and neutrino background spectra is worsened - independent of particle physics - once astrophysical uncertainties are taken into account [45].

Given that the next generation of ton-scale experiment is expected to become sensitive to coherent neutrino-nucleus scattering, it is pertinent to search for alternative and more powerful methods of subtracting the background. The most basic approach to alleviate the background is to exploit the complementarity between target nuclei of differing masses and nuclear content. For the SI neutrino floor it has been shown that this approach only leads to a marginal improvement in alleviating the neutrino background, however in the case of SD interactions the differences in nuclear spin contents make complementarity a more viable strategy [42]. It was also shown by Davis [46] that the use of timing information also allows the low mass neutrino floor to be overcome with slightly lower statistics. This approach exploits both the annual modulation of the dark matter signal due to the relative Galactic motion of the Earth and the Sun, as well as the annual modulation in the Solar neutrino flux due to the eccentricity of the Earth's orbit.

Directionality presents by far the most attractive prospect for circumventing the neutrino floor because the unique angular signatures of both dark matter and Solar neutrinos allows optimum discrimination between signal and background. This was first shown in Ref. [9] in the context of conventional low pressure gas TPCs and in Ref. [10] for experiments using a range of readout strategies. The effect of directional information has also been explored in ideas using nuclear emulsions [47] and spin-polarised helium-3 [48]. The general consensus is that in an idealised directional experiment there is effectively *no* neutrino floor. The crucial factor that enables this is that over the course of the year the Sun does not pass through the constellation of Cygnus. The angular distance between Cygnus and the Sun undergoes a sinusoidal modulation which peaks in September at around 120° and is a minimum during March at around $\sim 60^\circ$. Because Solar neutrino recoils can only point with angles less than 90° from the Solar direction, this implies that over long periods during a year there are large WIMP signal regions across the sky where it is guaranteed that the number of Solar neutrino events is zero (ignoring the effects of angular resolution). On the other hand, the advantage of directional detectors for dealing with the neutrino floor at higher masses is not as significant due to the greater angular dispersion exhibited by the remaining backgrounds [10]. The directionality of non-Solar neutrinos is much less well understood. Whilst the DSNB is certainly expected to be isotropic, one would not naively expect the same to be true for atmospheric neutrinos. Indeed FLUKA simulations of low energy neutrinos have shown an enhancement in the flux towards the horizon [49, 40]. However, for the atmospheric neutrino floor this phenomenon turns out to be unimportant in part because the directionality is fixed in the reference frame of the detector, as opposed to the Galactic signal which transits across the sky over a sidereal day. Additionally the coherent scattering process acts to wash out much of the horizontal directional preference meaning the recoil sky due to atmospheric neutrinos is also very close to isotropic in appearance. So directionality is much less powerful at circumventing the neutrino floor beyond 100 GeV, however an ideal directional detector can still out-perform an equivalent conventional experiment by a factor of a few.

2.1.3. WIMP astrophysics

[KM, COH]

A wide range of observations across Galactic to cosmological scales present strong evidence for the existence of dark matter as an unseen component of the Universe and a dominant contribution to the mass budget of galaxies, clusters, and the cosmic web. From measurements of the gravitational potential within the Milky Way, we can infer the distribution of dark matter locally and begin to reconstruct the full dark matter halo. While estimates of the local density of dark matter (within a few kiloparsecs of the Sun) have converged around a value of $\rho \approx 0.008 M_{\odot}\text{pc}^{-3}$ (see, e.g., [50, 51]), there is still a great deal of uncertainty surrounding the velocity distribution of the dark matter [52, 53], which impacts the direct detection rate via the distribution function $f(\mathbf{v}, t)$, as well as the motion of the Sun through the halo [54].

Astrophysical uncertainties impact the reliability of signal modelling and hence feed in to the measurements of dark matter particle properties [55, 56] and the calculation of exclusion limits [57, 45]. However the presence of these uncertainties presents an opportunity for discovery via directional dark matter detection due to the limitation of detection via the conventional means. It has been shown that the prospects for directional detectors to measure the dark matter velocity structure greatly exceeds that of an equal-standing *non*-directional detector [11, 58, 59]. This is primarily because with recoil energy information alone cannot be used to access the full three dimensional form of $f(\mathbf{v})$ and is instead only sensitive to the one dimensional speed distribution. It should be emphasised however that the structure of local halo of the Milky Way is also of great interest. The measurement of anisotropies in the velocity distribution may provide insights into the formation archaeology of the Milky Way, as well as the fundamental properties of dark matter. In particular, directional detectors are well suited to detect kinematically localised substructures such as dark matter streams [60] such as the nearby Sagittarius stream [61]. While very massive streams can be seen indirectly via studies of disrupted stellar systems, small streams and low-mass dark matter halos are likely to have undetectable levels of influence on luminous matter; an opportunity to better understand the level of clumpiness of the Milky Way dark matter halo is a key potential advantage of directional detection. However, less prominent velocity substructures such as debris flows [62] as well as low levels of triaxiality or asymmetry will require many more events to detect [63], hence very large directional detectors will be essential.

Any insight we may gain into the small-scale structure of dark matter halos has the potential to produce hints of non-vanilla dark matter models (such as warm dark matter, self-interacting dark matter, etc.) and to illuminate structure formation processes. It also has the potential to be fully unique probe, as there are currently very few observational handles on the small-scale structure and mass function of dark matter. The main limiting factors in the ability of directional detectors to constrain WIMP astrophysics are the precision obtained on the incoming direction of particles and the energy distribution of recoils [11]; we discuss the experimental prospects for direction and energy precision in Sections 3 and 4.

2.1.4. Particle models and directionality

[KM, COH]

As well as simply detecting dark matter, we also require that a future large-scale experiment be able to uncover properties of the particle itself. This is particularly challenging as there are many competing models that may be degenerate with respect to the signals they produce in the usual direct detection schemes. For instance it has been shown that various classes of particle models give rise to unique directional signals that would go undetected in a conventional experiment. We outline a few of these here.

Inelastic dark matter (IDM) models are those in which dark matter can have a lower or higher energy excited state that it can up- or down-scatter to after a nuclear recoil event. IDM models were proposed to reconcile the DAMA annual modulation signal [64]. The availability of excited states and the suppression of elastic scattering means that heavier nuclei are favoured, the low energy recoil spectrum is modified and the annual modulation is enhanced. It has also been shown that inelastic dark matter models can give rise to enhanced signal discrimination power in directional detectors [65]. This is because the recoils are more focused in the forward direction because slower WIMPs can not scatter with enough energy to induce an excited state. Directional detectors can also disentangle elastic and inelastic scattering events in dark matter models allowing for both [66]. Another possibility is if dark matter exists in the form of 'darkonium' bound states composed of two or more particles (as is predicted in some configurations of asymmetric dark matter models) it has been shown that there may be angular signatures observable in directional experiments that can constrain their properties [67].

Recently a novel scheme for describing non-standard signals in direct detection experiments was developed using non-relativistic effective field theory. The new framework proposes a set of additional set of operators beyond the simple spin-independent and spin-dependent, that include all Hermitian, Galilean and rotation-invariant interactions constructed out of the low energy degrees of freedom involved in the WIMP-nucleus interaction [68]. Certain examples, those which are dependent on the transverse velocity of the interaction, give rise to unique ring-like angular signatures [69, 70]. This means that directional detectors are potentially more powerful than conventional experiments in distinguishing between these particular operators. Furthermore these non-standard operators have suppressed interactions meaning event rates are inherently low. Large scale detectors will be essential for detecting dark matter if these interactions turn out to be the most important.

2.1.5. Axions

[COH]

Direct detection experiments searching for WIMPs are not limited to a single class of dark matter candidate. Arguably second most popular class of candidate is the axion and its generalization, the axion-like particle (ALP). The motivation for axions originates in the popular solution of Peccei and Quinn [71] to the strong-CP problem of QCD, see e.g. Ref. [72] for a review. The ALP is inspired by the QCD axion but may have a variety of different theoretical origins, most notably from string theory [73]. The masses of axions and ALPs can span many orders of magnitude but their stability and non-baryonic nature make them attractive dark matter candidates. Axions produced non-thermally in the early Universe via vacuum misalignment [74, 75, 76], decaying topological defects [77, 78] or in the form of axion stars [79] or miniclusters [80, 81] ensure that they can match the required properties and cosmological abundance of cold dark matter (see e.g. Ref. [82]). Axions and ALPs are by construction coupled to the standard model through quark loops which gives rise to a number of potentially observable interactions for example axion-photon conversion inside magnetic fields, absorption by atomic electrons (the axioelectric effect) and spin-precession of nuclei [83]. In the case of the QCD axion the strength of the coupling and its relationship to the axion mass is prescribed by the theory, however for the generalized ALP the coupling may take any value.

Existing WIMP direct detection experiments such as LUX [84], Xenon100 [85] and PandaX [86] have already constrained axions and ALPs in the search for their interactions with electrons via the 'axioelectric effect' an analogue process to photoelectric absorption [87, 88]. The coupling accessible to a WIMP experiment is therefore the axion-electron coupling, as opposed to the photon coupling measured in conventional resonant cavity searches such as ADMX [89] and CAST [90].

Axions may be probed as both a dark matter candidate as well as a modification to the standard model. If axions are believed to comprise a significant fraction of the local dark matter density then they should stream into a detector and induce electron emission from target atoms with a sharp spectrum located at the axion mass. On the other hand, even if axions are not dark matter, it is expected that they should be produced in the Sun with~keV energies. WIMP direct detection experiments will be able to observe these axions as well and their precise incoming flux and spectrum is understood [91]. As is the case with Solar axion telescopes such as CAST, if the ALP mass is much less than a keV then the signal is dominated by the energy of the Solar emission meaning an experiment is coherently sensitive to a large range of small masses. A large directionally sensitive experiment could be novel with respect to the detection of axions and ALPs because as with WIMPs there may be unique angular signatures. Although in the case of the axioelectric effect this is yet to be studied in detail and would require the directionality of emitted electrons at the relevant energy scales to be accurately reconstructed.

2.2. Neutrinos

[PB, KS]

2.2.1. Coherent neutrino-nucleus scattering

Coherent scattering between neutrinos and nuclei was predicted over 40 years ago with the realization of the neutral weak currents [92]. This standard model process went unobserved for many years due to daunting detection requirements: ~keV nuclear recoil thresholds, kilogram to ton-scale target masses, and low backgrounds. Recently however the COHERENT experiment made the first measurement of this interaction [93]. Due to the small weak charge of the proton, the coherence results in an enhanced neutrino-nucleon cross-section that is approximately proportional to the square of the number of neutrons in the nucleus. A few years after the coherent neutrino scattering prediction, and, ironically, before the conception of the first dark matter direct detection experiments, the possibility of using this enhanced process to develop a "neutrino observatory" was put forward [94]. A cornucopia of physics searches were envisioned using neutrinos from stopped-pion beams, reactor neutrinos, supernova, solar neutrinos and even neutrinos of a geological origin.

Shortly thereafter, the first generation of dark matter experiments began to search for the scattering of WIMPs of their detectors, where the signature was a low-energy nuclear recoil. These experiments have dramatically improved their sensitivities over the last three decades by simultaneously increasing the target masses, as well as reducing background nuclear recoils. Today the irony lies with the fact that the unshieldable recoils that result from coherent neutrino scattering will soon be a source of background for the next generation of dark matter direct detection experiments [36, 95, 37, 96]. Without the ability to separate the neutrino recoils, the progress in WIMP detection sensitivity will be halted. On the other hand, an experiment that can successfully separate and identify these neutrino events can not only proceed past the neutrino floor, but can also realize the long-awaited vision of a "neutrino observatory". A detector with directional sensitivity has the potential to do just that.

In the coherent neutrino scattering process, coherence is only satisfied when the initial and final states of the nucleus are identical, limiting this enhancement to neutral current scattering. The coherence condition, where the neutrino scatters off all nucleons in a nucleus in phase, is also only maintained when the wavelength of the momentum transfer is larger than that size of the target nucleus. Full coherence for all scatters is only guaranteed for low energy neutrinos – less than 10's MeV, depending on the target size. The standard model total cross section for the process can be approximate (neglecting neglecting axial vector terms that arise from unpaired nucleons):

$$\sigma = \frac{G_F^2}{4\pi}\left[Z(4\sin^2\theta_W - 1) + N^2\right]E_\nu^2|F(q)|^2 \tag{6}$$

Where G_F is the Fermi constant, Z is the number of protons, N is the number of neutrons, θ_W is the Weinberg angle, q is the momentum transfer, E_ν is the energy of the nucleus and θ is the scattering in the lab frame. It is evident that the cross section also increases with the square of the energy of the neutrinos; however, while the form-factor condition–which comes in as $|F(q)|^2$– is easily satisfied for Solar neutrinos, the total cross section begins to suffer from decoherence with supernova neutrinos, and neutrinos from stopped pion beams. A detector with an energy threshold of zero can expect to see several hundred to a few thousand recoils from solar neutrinos per ton-year of exposure, depending on the target mass [94].

The differential cross-section with recoil energy can be approximated as:

$$\frac{d\sigma}{dE_{rec}} = \frac{G_F^2}{8\pi}\left[Z(4\sin^2\theta_W - 1) + N^2\right] M\left(2 - \frac{E_{rec}M}{E_\nu^2}\right) \tag{7}$$

Where E_{rec} is the recoil energy of the target nucleus, and M is the mass of the target nucleus. Assuming a ^{19}F target, for example, and a 5 (10) keV threshold for observing nuclear recoils. This results in an expectation of ~90 (15) background recoils per ton-year, from solar neutrinos alone [95].

2.2.2. Solar neutrinos

The most prominent source of neutrinos is our Sun with a total flux at Earth of 6.5×10^{11} cm^{-2} s^{-1} [97]. Due to the eccentricity of the Earth's orbit, the Earth-Sun distance has an annual variation leading to a modulation in the Solar neutrino flux Φ,

$$\frac{\mathrm{d}^2\Phi(t)}{\mathrm{d}E_\nu \mathrm{d}\Omega_\nu} = \frac{\mathrm{d}\Phi}{\mathrm{d}E_\nu}\left[1 + 2e\cos\left(\frac{2\pi(t - t_\nu)}{T_\nu}\right)\right]\delta\left(\hat{\mathbf{r}}_\nu - \hat{\mathbf{r}}_\odot(t)\right)\,, \tag{8}$$

where t is the time from January 1st, $e = 0.016722$ is the eccentricity of the Earth's orbit, $t_\nu = 3$ days is the time at which the Earth-Sun distance is minimum, $T_\nu = 1$ year, $\hat{\mathbf{r}}_\nu$ is a unit vector in $\mathrm{d}\Omega_\nu$, and $\hat{\mathbf{r}}_\odot(t)$ is a unit vector in the inverse of the direction towards the Sun. The directional event rate is found by convolving this directional flux, with the directional cross section for coherent neutrino-nucleus scattering. The cross section with respect to the recoil angle can be written as:

$$\frac{d\sigma}{d(\cos\theta)} = \frac{G_F^2}{8\pi}\left[Z(4\sin^2\theta_W - 1) + N^2\right] E_\nu^2(1 + \cos\theta) \tag{9}$$

The resulting recoils are thus biased to the forward direction, away from the location of the Sun. As the solar position changes diurnally with respect to the expected direction of the WIMP wind, an analysis of the recoil direction of events in the detector should reduce the impact of this background. A similar separation could be imagined for terrestrial, atmospheric and diffuse galactic supernova neutrino backgrounds–each with their own characteristic directionality and energy scale.

The spectra of Solar neutrinos $\mathrm{d}\Phi/\mathrm{d}E_\nu$ come in various distinct forms depending on the nuclear fusion reaction involved in their production. Neutrinos from the initial proton-proton fusion reaction, *pp*, make up 86% of the Solar emission [98]. Despite the huge flux of *pp* neutrinos they yield nuclear recoils well below the threshold of any direct detection experiment, however they would be the dominant source of electron recoils. Secondary fusion of $p + e^- + p$ and ^{3}He $+$ p produce neutrinos, labelled *pep* and *hep*, extend to energies beyond *pp* neutrinos but with lower flux. There are also two monoenergetic lines associated with ^{7}Be electron capture with energies of 384.3 keV and 861.3 keV. The latter of these is principally responsible for limiting the discovery for $m_\chi < 1$ GeV [99]. At higher energies we have neutrinos due to the decay of ^{8}B which extend up to ~10 MeV in energy placing them within the reach of nuclear recoil WIMP searches, as already discussed. Finally the highest energy neutrinos emitted by the Sun are those arising from the carbon-nitrogen-oxygen (CNO) cycle labelled by the decay from which they originate: ^{13}N, ^{15}O and ^{17}F. These are at present unmeasured, but Borexino places an upper bound of $< 7.7\times10^8$ cm^{-2} s^{-1} on the sum of their fluxes [100].

The theoretical uncertainties on the Solar neutrino fluxes range from 1% (*pp* flux) to 14% (^{8}B flux). Although out of these various components, four have now been directly measured: *pp*, *pep*, ^{8}B and ^{7}Be. For all except ^{8}B, the theoretical uncertainty is smaller than the measurement uncertainty. The theoretical uncertainty originates largely from the uncertainty in the Solar metallicity, and in order to establish a self-consistent set of Solar neutrino fluxes one must assume a metallicity model. The Standard Solar models (SSMs) of Grevesse & Sauval [101] are generally split into two categories 'high-Z' and 'low-Z' based on the assumed Solar metallicity, Z. Both models have historically disagreed with some set of observables such as neutrino data, helioseismology or surface helium abundance [102]. The most recent generation of SSMs from Vinyoles *et al.* [103] have a mild preference towards a high-Z configuration, though neither are free from some level of disagreement with the various Solar observables. Dark matter detection experiments may shed further light on the Solar metallicity issue, e.g. Refs. [104, 99, 105]. The measurement of CNO neutrinos will be essential for this, and may be possible in future dark matter experiments [105]. The advantage of directional detection in performing these science goals is, as with dark matter searches, the vastly improved background rejection capabilities.

2.2.3. *Science with source and detector*

Stoppen pion neutrino source...

2.2.4. *Supernovae*

[KS] A core-collapse supernova will emit an enormous fluence of neutrinos over a few tens of seconds time scale. The neutrinos in the burst will have a few to a few tens of MeV of energy, and will include all flavors of neutrinos and antineutrinos with roughly equal luminosity [**?**]. Dark-matter detectors with very low recoil energy thresholds are sensitive to a supernova neutrino burst via coherent elastic neutrino-nucleus scattering. The order of magnitude is a few events per ton of detector material for a supernova at $\sim$10 kpc (near the most likely distance to the supernova [**?**]), and statistics will scale linearly with detector mass and as the inverse square of distance to the supernova. Such a detection would be valuable due to its sensivity to the entire flux, given that most other detectors online are sensitive primarily to the $\bar{\nu}_e$ (in water, scintillator detectors) and ν_e (in argon, lead detectors) components of the flux [106]. Furthermore, some neutrino spectral information can be reconstructed from the measured nuclear recoil spectrum.

The advantages of directionality for the detection of supernova burst neutrinos via CEvNS are several: first, obviously, directional information about the source will be of value to observers in electromagnetic wavelengths and in gravitational waves who want to make prompt observations of the supernova event in real time. Currently, only detectors able to make directional measurements of elastic scattering on electrons have good pointing ability (and Super-K is the only current instance). Even if there is no obviously bright supernova event (as may be the case for a failed supernova), directional information will be able to narrow down the possible progenitors. Finally, the direction information can be used on an event-by-event basis to reconstruct an more precise neutrino energy.

Diffuse supernova neutrino background as a test of cosmology? [39, 107].

Detecting/pointing Galactic SN as in Ref. [108].

2.2.5. *Atmospheric neutrinos*

Atmospheric neutrinos, low energies still hard to measure [41].

2.2.6. *Geoneutrinos*

Geological neutrinos...? From Sven: yes, please. Here's the reference: [109]

2.2.7. *Exotic models*

Dark matter experiments will also be able to explore novel neutrino sector physics. The recently measured coherent neutrino-nucleus scattering cross section [93] appears to agree with the standard model prediction currently. However it may be that there are additional non-standard interactions that would affect the recoil energy spectra observable in future dark matter experiments. For example Ref. [105] explored the prospects for future ton-scale experiments to perform novel Solar neutrino physics, such as measuring the pp or ^{8}B flux, as well as constrain the running of the electroweak mixing angle and the possible existence of additional mediators from some light dark sector. Additional exotic interactions involved with both dark matter and neutrinos may also affect the shape of neutrino floor [110], for which directional experiments will be needed. It was also shown in Ref. [104] that direct detection experiments would be able to make complementary constraints on sterile neutrinos if both coherent nuclear and electron scattering of Solar neutrinos is measurable. Again, the strong directional signature from Solar neutrinos means that a directionally sensitive experiment may be very constraining if scaled up to large target masses.

3. Existing Directional Detection Technologies

[Section organizer: James Battat]

Contributors to this section:

- James Battat jbattat@wellesley.edu
- Elisabetta Baracchini baracch@gmail.com (esp. with "emerging tech." such as columnar recombination, nanotubes, anisotropic scintillators, DNA, etc.)

Directional detection can be achived by a direct reconstruction of the nuclear recoil geometry (e.g. by building a tracking detector), or by an indirect proxy for the recoil direction (*e.g.* a detector whose response depends on the relative alignment of the recoil and the detector axes). A detailed and critical assessment of directional readout technologies is provided in Ref. [111].

3.1. Detectors that reconstruct the recoil track

The currently active directional experiments all aim to reconstruct the geometry of the recoil track. Of these, most make use of a low-pressure gas Time Projection Chamber (TPC), in which the track geometry is measured in 1D or 2D or 3D. In addition to gas-based TPCs, track reconstruction at the FIXME sub-millimeter scale has been demonstrated in solid emulsions. More exotic and at this point unvalidated technologies such as a customized matrix of DNA strands have been proposed as well.

3.1.1. Gas-based TPCs

james will do this

- Negative ion drift vs. Electron drift
- amplification device may be integral to readout (micromegas, MWPC) or separate (GEM)
- MWPC
- MPGD (micromegas, mupic, pixel chip)
- Optical

3.1.2. Nuclear Emulsions

James will populate this

[112]

see also EB's excerpt.

3.1.3. DNA strand detector

A highly novel recoil tracking detector makes use of customized DNA or RNA strands mounted in a matrix onto a nanometer-thick gold foil [113]. A WIMP would interact with and kick out a gold atom from the foil, and the recoiling gold atom would sever several DNA strands. Using well-established biological techniques such as polymerase chain reaction (PCR) and sequencing, it would be possible to identify the (x, y, z) coordinate of each severing event, thereby reconstructing the nuclear recoil axis (though not the vector direction). Originally proposed in 2012, there are no published experimental demonstrations of this technology.

3.1.4. Planar targets (graphene)

Nuclear recoils in a 3D (bulk) target suffer multiple interactions with the surrounding medium that scramble the recoil direction. In principle, the recoil direction can be more directly measured if the target is planar. Furthermore, planar targes can be fabricated from semiconductor materials in which the exictation energy is on the order of $\sim$ 1 eV, allowing even MeV-scale WIMPs to initiate electronic excitations. A recent proposal [114] suggests that 2D graphene could serve as a directional detector of sub-GeV WIMPs. This is a particularly interesting idea, especially given that no other directional technology can probe this WIMP mass scale. Although there has not been an experimental demonstration of this technology, it may be possible to do so within the PTOLEMY experiment (a relic neutrino search) [115].

3.2. Detectors that indirectly determine the recoil direction

3.2.1. Anisotropic scintillators

Solid scintillators (*e.g.* NaI and CsI) are commonly used in particle detection, and specifically in dark matter detection. Because of their large target mass and high-A content, they are particularly interesting for spin-independent WIMP searches. Some scintillators, such as $ZnWO_4$ and stilbene have been shown to exhibit a response that depends on the recoil ion direction relative to the crystal axes. In principle, this scintillation anisotropy can be used to infer the nuclear recoil track direction without direct reconstruction of the track geometry. Several groups have explored the possibility of using anisotropic scintillators for a directional dark matter search [116, 117, 118, 119, 120, 121], though the magnitude of the anisotropy is too small for a sensitive directional WIMP search.

It is important to notice that none of this have yet proven anisotropic scintillation for low energy nuclear recoils. Therefore, all the quoted energy resolution, threshold and general performances are for general detection of alpha, beta and gamma radiation and not necessarily valid for nuclear recoils.

3.2.2. Columnar recombination

When heavy tracks ionize a medium, a column of electrons and ions gets created along the track direction. If no electric field is present, these particles will recombine producing a scintillation light signal. Since recombination probability depends on the proximity of electrons and ionized atoms, if an external electric field is applied, the amount of light produced will depend on the relative orientation of the field with respect to the ionizing track. A large angle, in fact, will lead electrons transversely away from the ions, generating a small recombination scintillating signal (R), while a small angle will bring electrons and ions closer together and produce a relative enhancement of the R signal with respect to the ionization signal (I). A precise measurement of the R/I ratio (charge/light) could therefore be used to ?sense? the directionality of the track without actually seeing it [122]. Since the direction is inferred from this ratio that is produced prior to the drift, all the limitations imposed by the degrading effects of diffusion, avalanche gain and reconstruction noise would be effectively largely reduced, possibly allowing the construction of large monolithic Xenon gas TPC at the ton-scale. With the Xe density at 10 bar being 0.05 gr/cm^3, a 1-ton detector could be realized with only 20 m^3.

Evidence for columnar recombination in alpha tracks was observed in dense Xenon [123], so the question still to be answered is if this can be seen for the much shorter nuclear recoils. Recent simulations [124] confirm how, with the proper cooling of the ionized electrons, the recombination probability should show directional sensitivity for track longer than about 2 μm in gaseous Xe at 10 bars, implying about 30 keV energy threshold. The main issue is to keep electrons thermalized near the ions in order to recombine efficiently, but unfortunately pure Xe do not satisfy this requirement due to the lack of inelastic scattering below 7 eV. This is the reason why the only only published work on the subject employed Trimethylamine (TMA) as dopant, because of its large inelastic cross-section, its UV-quenching properties and the possibility of exploiting a Penning effect. The transformation of the Xe^+ image into the TMA^+ molecular image and the columnar recombination happening on TMA^+ ions would then provide light around 300 nm, a much more PMT-friendly light than the Xe emission spectrum. Unfortunately, despite enhancement of recombination with TMA was observed, no sign of scintillation light from recombination was detected and TMA was found to highly absorb Xe light without re-emitting it [125]. The use of alternative dopants, possibly generating negative ions drift, has recently been suggested but not yet tested.

While columnar recombination is intrisically sensitive to the axial track direction but not to its sense, the combination of two detector with the drift fields anti-aligned could be able to show head-tail sensitivity in a statistical way. The final performances of an experiment based on this technique, in terms of energy threshold and resolution, directionality performances and efficiencies, will highly depend on the readouts chosen to detect the light and charge produced in the process, and is therefore beyond the possibility of evaluation as for today.

3.2.3. Carbon nanotubes

Single wall aligned carbon nanotubes (CNTs) have been recently proposed as a DM target due to their an anisotropic response to neutral particles [126]. When a C ion gets scattered off the CNTs walls, in fact, if the right initial conditions are met, it sees the tube as empty and can travel with nearly no loss of energy (i.e. channeling). Numerical simulations have confirmed that different orientation of the CNTs axis with respect to the Cygnus constellation would give sensibly different channeling probabilities and therefore produce significantly different C ions current at the end of the nanotube.

The proposed detector concept by [126] is a brush of CNTs array closed at one end and opened at the other, inserted in a (low-pressure) TPC to detect the outgoing C ions down to low $\sim$ 10 keV. An R&D effort is currently on-going in Italy to test the channeling hypothesis for neutral particle scattering and the TPC detector approach. If these were proven successful, then an experiment based on this technique would profit from the higher density of CNTs (seems possible to reach about 10 kg on 100 thin stacked CNTs panel of 1×1 m^2 each) and possess about the same performances of a gaseous TPC-based approach, depending on the chosen readout. Other possible detector configuration (with solid target to detect the outcoming C ions, for example) could also be considered and would show significantly different performances.

3.3. Summary table

Requires a bit of thought...

- Energy resolution demonstrated.

- Axial reconstruction demonstrated? Down to what energy? With what angular resolution?
- Sense-recognition demonstrated? Down to what energy?
- Full-volume fiducialization demonstrated?
- Flexibility for different targets (mostly for gas-based TPCs – e.g. different gases, negative ion vs. electron drift)
- Technological readiness (including largest volume in operation, prospects for scaling up, some mention of cost per something (e.g. volume, or area, or ....)
- Background discrimination? This would potentially be a rather hard item to cover... gamma/recoil separation studies by Loomba et al.

  NEWAGE: 1e-6 at 50keVee at 100 Torr (CF4)

  DRIFT: 2e-7 above 30keVr at 41 Torr (CS2:CF4:O2)

  MIMAC: ???

  Pixel chips: ???

  Dinesh: ???
- background level studies of material / components - perhaps already covered by Neil?

4. Comparison of Directional WIMP and Solar Neutrino Sensitivity

[Section organizer: Sven Vahsen]

This section compares the directional sensitivity of different TPC readout technologies to key science goals, such as discovering a WIMP signal pointing back to CYGNUS, and using the detected recoil angle distribution to distinguish or separate a WIMP signal from a neutrino signal. These comparisons incorporate cost, as the ideal detector is the one the maximized science sensitivity per unit cost. We also estimate electron rejection factor versus energy of each technology. We assume here that zero background is achievable with each technology. That assumption is explored further in section 5, where the impact of the electron rejection factors is discussed. As discussed in section 2.1.2, reference [10] has already compared the ability of detectors with 1-d, 2-d, and 3-d readout dimensionality to detect a WIMP signal below the neutrino floor. Here we aim to go one step further, by simulating specific readout technologies from the ground up. By simulating irreducible detector effects such as diffusion of drift charge and readout noise, we obtain a more realistic, energy dependent description of the detector performance. For instance, the angular resolution for nuclear recoils becomes energy dependent, and the head-tail (i.e. vector) sensitivity turns on softly at a readout-dependent energy threshold. Existing directional detectors were already discussed in section 3. Our goal here is not to compare specific experiments, but rather available technologies, which could be used in future experiments. Hence we focus on gas TPCs, which are the furthest along in terms of technological readiness. The performance of these detectors has been studied extensively, allowing us to performance simulation and ensuring our our comparison is realistic. Comparing TPCs against other approaches is also important, and may still be included here, if time allows.

4.1. Simulation

The simulation of directional detectors used here consists of the following stages: momentum vector generation, generation of nuclear recoil and electron ionization distributions, simulation of the charge propagation in the detector, simulation of the detector readout, track fitting and final analysis. Each stage is described below.

4.1.1. Momentum vector generation

WIMP recoil vector are generated using the Standard Halo Model (SHM), where the dark matter is modeled as an isotropic, isothermal sphere with circular velocity $v_0 = 220$ km/s and escape velocity $v_{\rm esc} = 533$ km/s and a dark matter density of $\rho_0 = 0.3$ GeV/cm^3 at the detector. The form factors used are .... In transforming the recoils to lab coordinates, (unless explicitly stated otherwise), the detector lattitude and longitude are taken to be those of Boulby, England. Recoils are distributed uniformly in time over one year, and spatially uniformly in the detector. Electron momentum vectors are generated uniformly in the detector and isotropically with respect to the detector coordinate system.

4.1.2. Nuclear recoil and electron event generation

To simulate nuclear recoils and electron events, we utilize the event generators SRIM [127] and DEGRAD [128], respectively. Both generators take as input the momentum vector of the particle to be simulated, and configuration files that specify the gas mixture. SRIM then outputs a 3-d distribution of energy lost to ionization, while DEGRAD outputs a 3-d distribution of ionized electrons. Figure 2 shows examples of generated events, and Figure 3 shows properties of the generated events versus energy, for two gas mixtures.

Figure 2: Examples of generated events. Left: 10 keV_{ee} Flourine recoil in 20 torr of SF_6 gas, generated with SRIM. Right: 10 keV_{ee} electron event in 20 torr of SF_6 gas, generated with DEGRAD.

Figure 3: Range, quenching factor, and stragling of Flourine recoil and electron events in SF_6 gas, versus ionization energy.

4.1.3. Simulation of detectors and readouts

After generating charge clouds as described above, we simulate the drift of ionization in TPCs using the parameters in Table 1. These parameters only depend on the target gas being simulated, and are common for all readouts, to ensure a fair comparison. Note that the common parameters include the same avalanche gain and gain resolution for each readout. This means that we are comparing detectors with the same gain stages, but different charge readout technologies. While many other combinations are possible, keeping the gain stage fixed allows us isolate the effect of each readout on the final performance. The subsequent detection of drift charge is simulated using the readout specific parameters shown in Table 2.

Table 1: Gas-dependent parameters used in the TPC detector simulation.

Gas mixture	SF_6	SF_6:He	SF_6:He
Gas pressure [torr]	20	60:20	600:200
W [eV / ion pair]	35.45		
Avalanche gain	9000		
Gain resolution, σ_G/G [%]	20		
Transverse diffusion, σ_T [$\mu m/\sqrt{cm}$]	116.2		
Longitudinal diffusion, σ_z [$\mu m/\sqrt{cm}$]	116.2		
Drift velocity [μm/μs]	140		
z binning (assume 1MHz sampling)	140		

4.2. Directional power of detectors versus recoil energy

The final detector comparison is sensitive to astrophysics, gas optimization, detector performance, and cost. To decouple these effects, we here start out by quantifying directional performance versus recoil energy. This is done by estimating how many recoils each detector needs to observe, to discriminate a delta function (all recoils go in the same 3D direction) at 5-sigma from a flat recoil distribution, versus recoil energy. This goal here is to provide an intuitive result that clearly shows the recoil energy range where each technology is effective, and how directional it is.

4.3. Directional WIMP and Solar Neutrino Sensitivity

Compared to the previous section, in this section, and the next, we now also fold in the recoil distributions for a realistic physics scenarios, target interaction probability, and cost. We explain how we compare the sensitivity of directional technologies, including how we optimize for nuisance parameters such as gas pressure. The procedure for one physics goal is explained in detail, culminating in a final publicity plot where directional detector technologies are compared against each other and against

Table 2: TPC readout technologies being simulated, and readout-specific parameters that are used in the simulation of each. The capacitance listed is that for a single detector element, which determines the noise level.

Readout type	Dimensionality	Segmentation ($x \times y$)	Capacitance [pF]	Noise in 1 μs [$e-$]	Threshold/Noise
planar GEM	1-d (z)	10 cm $\times$ 10 cm	3000	18000 e-	3
large pixels	1-d (z)	3 mm $\times$ 3 mm			
wires	2-d (yz)	1 m wires, 2 mm pitch		800	3
optical CMOS	2-d (xy)	200 $\mu m \times$ 200 μm - t.b.d.			
resistive strip Micromegas	3-d (xyz)	1 m strips, 200 μm pitch	500	2800	3
pixel ASIC	3-d (xyz)	200 $\mu m \times$ 200 μm	0.012 - 0.200	42	30

non-directional ones. Such a publicity plot is one key goal for the paper. A candidate example plot could be "# sigma that a galactic-coordinate dipole pointing back to CYGNUS, and a flat recoil distribution can be separated, per million dollars, for a 100 GeV WIMP" [with a specified cross-section]. Non-directional detectors probably score zero on this performance metric. If cost proves too hard to pin down, then we can instead show #sigma per cubic meter for each technology, chose a TPC with wires as the default, and tabulate the required cost for other technologies to become competitive.

4.4. *Figure of Merit for Specific Science Goals*

The same procedure as in the previous section is now repeated for a number of physics goals. Again, we'll ask Ciaran to generate the 3-vectors for nuclear recoils from WIMPs and neutrons. This time, only the final result (the publicity plot) is given for each physics goal.

Candidate list of physics scenarios (will be revised based on physics case chapter):

- discover DAMA/LIBRA WIMP
- discover 100 GeV WIMP above neutrino floor
- discover 1TeV WIMP above neutrino floor
- discover WIMPS below neutrino floor (1, 10, 100, 1000 GeV)
- discover WIMP streams

4.5. *Electron rejection factors*

4.6. *Optimization of gas pressure*

4.7. *Optimization of drift length*

4.8. *Optimization of detector segmentation*

4.9. *Conclusion on Technology Choices*

Follow this with discussion of optimal technology choices: Is there a general winner that emerges? Or one winner for high, and one for low energy recoil scenarios? Is the conclusion biased by the zero background assumption? How would it change if discrimination power is included? (Can we think of an easy way to do that?)

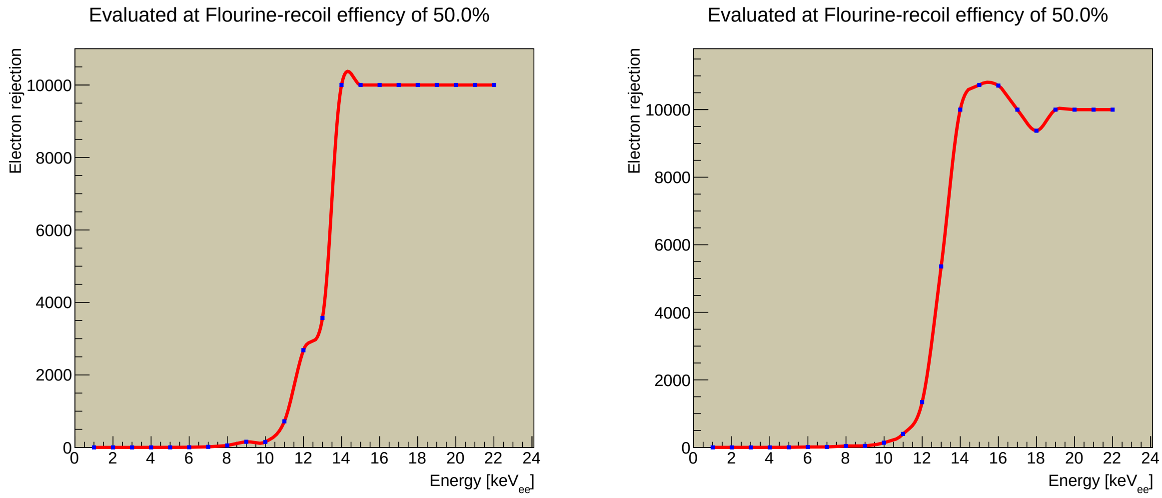

Figure 4: Electron rejection factor versus energy, for electron events with 3d readout, before (left) and after (right) diffusion of drift charge.

5. Zero Background Feasibility

[Section organizer: Neil Spooner]

Direct search dark matter experiments strive to control backgrounds sufficiently so as to achieve an expected rate of less than 1 background event recorded in the anticipated exposure time and target mass, essentially that we have zero background within the fiducial volume. An assumption that this is achievable for all the directional technologies compared here was an important caveat made in the previous section of this work. This next section now addresses the realities of this assumption. Specifically we seek to answer the question firstly whether or not directional low pressure gas TPCs can in principle achieve such low backgrounds at the experiment scale required to reach the proposed scientific goals, but further, whether particular TPC readout technologies, with their individual associated intrinsic backgrounds and discrimination capabilities, are more or less able to reach these goals. The latter aspect depends in part on assumptions about the radio-purity of internal detector materials likely involved, most notable for instance because this affects the total internal neutron background. So an alternative tack, adopted here also, is to estimate and compare the specification on material radio-purity required for success, for instance the ^{238}U content in each case, then to comment on the achievability of these requirements.

As shown in [ref x, Abbassi 2005] the additional particle identification properties of directional detectors mean that in principle they may in actuality be able to tolerate a non-zero level of isotropic nuclear recoil background, yet still be able to identify the signal of interest here for dark matter, a non-isotropic distribution of recoil directions. However, the level of tolerance will depend strongly on the capabilities of the technology and anyway will clearly reduce sensitivity overall. A maximum signal to background ratio of order 10 might be a reasonable upper limit in certain circumstances [ref ?]. Nevertheless, a good starting point for comparison purposes, adopted for this work, is to assume an aim of zero background.

The following sections present results and conclusions on these issues based on new Geant4 detector Monte-Carlo simulations of the various key background contributions. Although not necessarily mandatory, experience from many dark matter experiments demonstrates that full fiducialisation of the active detector volume is likely necessary to achieve the background goals. This aspect is addressed in 5.1. The fundamental issue of the neutron background, which results in nuclear recoil events likely indistinguishable from WIMP induced events, is addressed in 5.2, considering separately contributions from cosmic ray muon neutrons, and rock and detector neutrons. The subsequent parts cover respectively simulations of gamma, radon related backgrounds. For the majority of the technologies some generic conclusions can be drawn based on the commonality of the basic infrastructure needed for any TPC dark matter experiment, such as a deep site, passive shielding and containment vessel. The majority of any variance from this comes from details of the internal TPC structures, notably the readout planes. These aspects are together summarized in 5.6.

5.1. Fiducialization

5.2. Neutron Backgrounds

Neutrons are a major concern for all direct search experiments because they can produce nuclear recoils just like WIMPs. However, there are various issues that make the requirements for mitigating against neutron backgrounds in a low pressure gas TPC significantly different from those cases involving conventional solid or liquid based detector technologies. Firstly, the potentially low sensitivity to light charged particles, muons, muon-induced secondary particles and electrons, means that these may not be recorded. Secondly, the low density of the target means neutrons are less likely to undergo double or multiple scatters. Both these factors potentially reduce options for vetoing neutron induced nuclear recoils, depending on the readout technology chosen. The former does depend critically on the degree of position segmentation of the readout and the energy threshold achievable in those individual readout channels, essentially the sensitivity to $^{dE}/_{dx}$. The issue of vetoing by recording multiple neutron scatters then depends on the contiguous size of the detector array. For instance, at 200Torr SF_6, the mean free path of a typical background neutron is 60m. This would be the sort of scale required to have any benefit from detection of multiple neutron scatters.

Factors such as these, the uniqueness of the low pressure TPC technique and potentially powerful particle identification, mean that estimating neutron backgrounds by extrapolation from existing background simulations such as have been performed for massive xenon or bolometric detectors [Aprile 2013, arxiv 1306.2303v2 has a good description for XENON100], is not appropriate. The work presented here is thus based on a set of dedicated TPC Monte-Carlo simulations. Some relevant initial work on neutron backgrounds was previously undertaken by some of the authors here but focused on smaller TPC target masses of order $1 - 10$kg [This is the Cygnus24 paper ?]. The new work presented here makes use of the latest updated Geant4 and SOURCES packages and specifically targets the more complex situation of neutron background mitigation in the much larger experiments required to reach the goals of CYGNUS. As noted the procedure adopted is to start by examining aspects that are independent of the internal readout technology. This includes firstly the laboratory location, determined by the depth, rock composition and cavern geometry. Secondly, the outer passive shielding and any active veto system, and finally the containment vessel, modeling both its geometry and composition. The remit here is to investigate muon-induced neutrons resulting from cosmic-rays penetrating from the Earth's surface and also neutrons produced by spontaneous fission and alpha-n reactions in the rock and shielding/vessel materials. The procedure thus requires simulation of the geometry, particle production, tracking and detection, the goal being to find the rate of neutron-induced nuclear recoils anticipated in different situations. From this can be determined requirements for such issues as the amount of passive shielding, the efficiency and form of any external veto and the form and purity of the vessel materials, such as required to achieve the goal of zero background. The issue of neutrons from internal detector components, that depends on details of the readout technology, is addressed last.

5.2.1. Laboratory and TPC Geometry

Most parameters are independent of the location of the experiment, especially regarding the inner parts of the detector. Other parameters can be scaled to estimate the rate of background events at different laboratories. For these simulations, we concentrate on the background present in salt rock similar to the Boulby Underground Laboratory in the UK.

In the case of neutrons from (α, n) and spontaneous fission emanating from the rock, 3m of material were simulated on each side of the detector. As presented in 5, simulations have shown that the neutron flux saturates at this distance so neutrons produced beyond 3m do not actively contribute to the total neutron flux. For muon-induced neutrons, the thickness of rock is increased to 20m in order to fully allow the muons created at the surface of the geometry to decay.

In both case, it was assumed that no objects other than the vessel and its shielding are present in the cavern. The dimension of the vessel, however, depends on the materials from which it is made and the composition and pressure of the gas adopted for the experiment of which there are many possibilities. For the purposes of making broad comparisons here, bearing in mind the science goals of CYGNUS, it was decided to assume use of SF_6 gas at 50Torr with volume sufficient to produce around 0.5Ton of target nuclei, in this case of fluorine. In both case, a generic detector with an inner-volume of $10 \times 10 \times 10\mathrm{m}^3$ was modeled. Real vacuum vessels of such size will require strengthening supports both inside and outside. However, for simplicity in simulations the mass of these was taken into account by applying an appropriate average increase in thickness to the vessel walls.

As stated, the background from internal TPC components will be affected by details of the readout design, covered later. Nevertheless, some generic assumptions can be made about other TPC structures required inside the detector which are likely common to any design. Most notable here is the central cathode and field cage. However, we note that the total area required for the former will also depend on the gas mixture adopted, since this influences the diffusion and hence determines the maximum drift distance that can be tolerated. For the comparisons here we assume a compromise drift distance of 50cm, which yields a

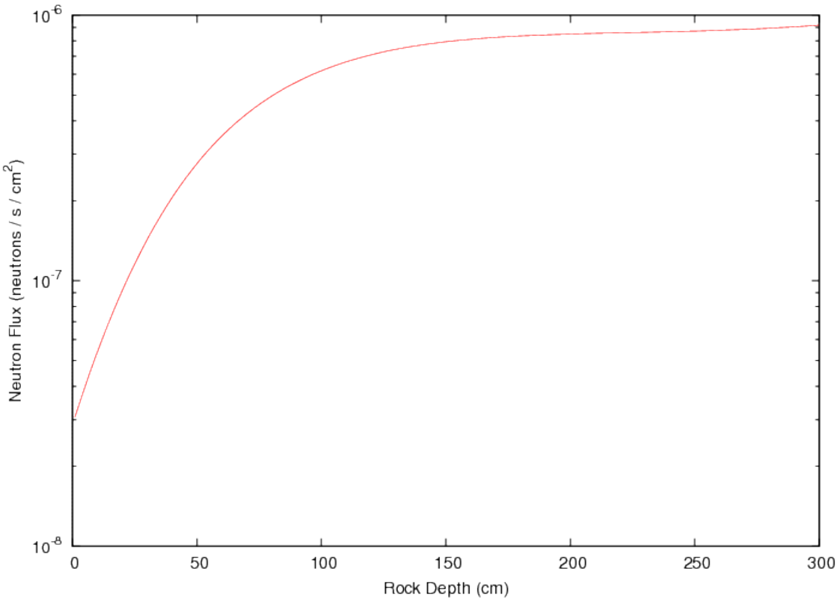

Figure 5: Rock neutron flux at Boulby as a function of depth

total cathode area of 2000m^2 in both options. The design of this is assumed here to comprise ultra-thin cathode sheets supported on acrylic frames. The field cage itself can also be made of light acrylic components, with copper strips to act as the field rings. In these components the acrylic provides by far the dominant mass, conservatively estimated to be 86.4 tons [1000xDRIFT]. The components are, in turn, approximated as sheets of appropriate thickness in the TPC to simulate their neutron yield. The thickness of the sheets is chosen such that it may account for self-shielding. Geant4 provides the option of homogeneously populate the material studied with the relevant primary particles. This option enables the simultaneous treatment of background originating from the bulk of materials, as well as surface background contamination.

5.2.2. Rock Neutrons and Passive Shielding

The first simulations were performed to determine what thickness of passive neutron shielding is required around the CYGNUS detector to ensure an induced recoil rate from this source that is below 1 per year. It is recognized that an active veto shield is also likely needed to assist with rejection of muon related neutrons (see 5.2.5) and that, in practice, this could be fully, or partially, integrated with the passive shield. The simulation varies the thickness of a water shield around all sides of the detector until the requirement of less than 1 background event per live-year is fulfilled. Possible contamination of the water by radionuclei was not simulated as measurement performed at Boulby for DRIFT showed that the level of contamination in clean, non-distilled water were on par with the levels already obtained with polypropylene pellets. Furthermore, it is assumed here that any containment structure or internal components, such as photomultipliers, are of sufficiently low background and low mass to be ignored. We note also that account needs to be taken of the energy threshold chosen, as determined in part by the science priorities. To allow for this we consider cases for a 1 and 10keV threshold.

For this work, SOURCES was used to generate neutrons from the U and Th decay chains in salt rock corresponding to the Boulby Underground Laboratory. The results obtained in this section can be scaled to different underground laboratories and additional shielding materials can always be added if required. SOURCES simulates the contribution to the ^{238}U chain from spontaneous fission using the Watt spectrum, while the (α, n) spectra are computed from the energy of the alphas and the related cross-sections, branching ratios for the different transitions between excited states, lifetimes of the isotopes and stopping power of the alphas in the modeled materials. The version of SOURCES used has been modified to extend the energy range considered from up to 6.5MeV originally to up to 10MeV using experimental data [Quote Carson ?].

6 shows the neutron energy spectra obtained for both decay chains at Boulby. We used Geant4 to randomly populate the rock with isotropic neutrons with energy sampled from the sum of spectra obtained with SOURCES. The simulation was repeated for various thickness of the water shield until the nuclear recoil rate in the gas was below the imposed limit. The results obtained

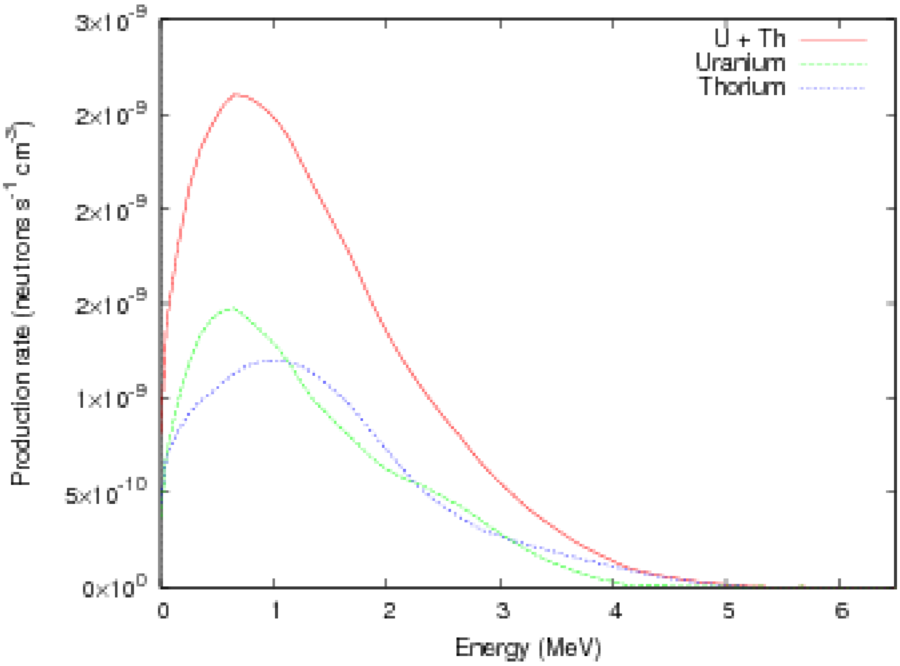

Figure 6: Neutron energy spectrum from the salt rock at Boulby

Water shield thickness	Nuclear recoil rate in salt rock
50cm	$(1.8 \pm 0.7) \times 10^{-6}$Hz
75cm	$\leq 2.96 \times 10^{-8}$Hz (90%CL)

Table 3: Nuclear recoil rates from rock neutrons above a 1keV$_r$ threshold as a function of shield thickness in salt rock

are summarised in Table1. Similar tests with Geant4 carried out by the authors have shown that there exists a linear relationship between the nuclear recoil rate in the detector and the pressure of the target gas so long the probability of double scattering of neutrons in the gas remains negligible. We have found this relationship to be true only for nuclear recoils. On the other hand, simulations of Compton scattering at different pressures have shown evidence for self-shielding from the gas at high pressure. To reduce the computational burden, simulations of the rock background were done at 600Torr, a factor 12 above the chosen pressure. We made sure that simulations performed at both the increased and nominal pressure indeed returned the same results. This shortcut is possible since low pressure gas TPCs can be made insensitive to gammas by increasing their threshold such that the lower dE/dx of electron recoils do not trigger the analysis. In each case, a separate simulation dedicated to the gamma background was performed at nominal pressure.

3 shows that 75cm of water shielding are required in order to reduce the neutron background in salt rock below 1 event per year. The concentration assumed were 70ppb $\left({}^{238}\text{U}\right)$ and 125ppb $\left({}^{232}\text{Th}\right)$ as reported in [Murphy, IDM2004]. We found that 70ppb of ^{238}U produced 3.5×10^{-8}neutrons/s/cm^3 with a mean energy of 1.74MeV, and that 125ppb of ^{232}Th produced 3.08×10^{-8}neutrons/s/cm^3 with a mean energy of 1.92MeV.

5.2.3. Vessel Neutrons

As seen in 5.2.2, the external rock neutron flux can be controlled by passive shielding. Neutrons from internal detector radioactivity are known to be a harder challenge since control of this likely relies on selecting radio-pure materials, use of tricky internal shielding or innovative analysis techniques. The vacuum vessel, being the component with by far the largest mass, has the potential to dominate this aspect, followed by the outer passive shield, TPC field cage, and resistors. Rather than assume values for the U and Th content of the vessel materials the approach taken here is to determine from the simulations what amount of U, Th contamination can be tolerated in the vessel without compromising the criteria of less than one event recorded per year,

	$1keV_r$ threshold		$10keV_r$ threshold	
shield thickness	U (ppb)	Th (ppb)	U (ppb)	Th (ppb)
0cm	$(4.910 \pm 0.004) \times 10^{-3}$	$(2.455 \pm 0.002) \times 10^{-3}$	$(6.537 \pm 0.006) \times 10^{-3}$	$(3.269 \pm 0.003) \times 10^{-3}$
10cm	$(2.709 \pm 0.007) \times 10^{-2}$	$(1.354 \pm 0.004) \times 10^{-2}$	$(3.96 \pm 0.01) \times 10^{-2}$	$(1.983 \pm 0.006) \times 10^{-2}$
20cm	$(8.1 \pm 0.1) \times 10^{-1}$	$(4.05 \pm 0.06) \times 10^{-1}$	1.14 ± 0.02	$(5.7 \pm 0.1) \times 10^{-1}$

Table 4: Maximum concentration of ^{238}U and ^{232}Th for a steel vessel with internal acrylic shielding

	$1keV_r$ threshold		$10keV_r$ threshold	
shield thickness	U (ppb)	Th (ppb)	U (ppb)	Th (ppb)
0cm	$(8.54 \pm 0.02) \times 10^{-4}$	$(1.422 \pm 0.003) \times 10^{-3}$	$(9.86 \pm 0.02) \times 10^{-4}$	$(1.644 \pm 0.003) \times 10^{-3}$
10cm	$(9.95 \pm 0.06) \times 10^{-3}$	$(1.66 \pm 0.01) \times 10^{-2}$	$(1.30 \pm 0.01) \times 10^{-2}$	$(2.16 \pm 0.01) \times 12^{-2}$
20cm	$(1.73 \pm 0.03) \times 10^{-1}$	$(1.73 \pm 0.03) \times 10^{-1}$	$(1.33 \pm 0.03) \times 10^{-1}$	$(2.21 \pm 0.05) \times 10^{-1}$

Table 5: Maximum concentration of ^{238}U and ^{232}Th for a titanium vessel with internal acrylic shielding

at each energy threshold. Given the potential difficulty of obtaining steel with low U, Th content, the simulation also considers acrylic and titanium vessels. For the steel and titanium vessels, we explore the possibility of including acrylic shielding inside the vessel to block neutrons emanating from the vessel. In this case, the acrylic inner-shield is assumed to be inert, but its neutron yield can be estimated from the simulation of an acrylic vessel. In order to deduce the maximum U and Th content possible, it is necessary to fix the ratio of the two. We used the UKDM database [ref of UKDM] to estimate the typical ratio of U to Th. This ratio seemed to vary greatly between samples, especially in the case of steel. In these situations, we chose a ratio which would correspond to a typical case, or to a known example. As such, a ratio of $C_U = 2C_{Th}$ was assumed for steel, roughly similar to the ratio in the DRIFT vessel stainless steel. In any case, these results should be considered as benchmark values in order to estimate the feasibility of building a large dark matter TPC detector rather than a full background simulation. Secular equilibrium is assumed for both the U and Th decay chains. Tables 2 and 3 summarise the results in terms of specifications on the maximum U, Th levels that can be tolerated in each scenario in order to obtain less than one nuclear recoil per year..

Some initial conclusions can be extracted from these results. Firstly, a large radio-assay was conducted for the LZ experiment [ref LZ paper] when several samples of steel were examined. Low-background concentrations were achieved at 0.08ppb ^{238}U and 0.12ppb ^{232}Th. This is a factor 10 improvement for U and 5 for Th compared to the DRIFT vessel (0.81ppb U and 0.51ppb Th) [ref UKDM]. However, similar concentrations were achieved in stainless steel by the GERDA group (0.081ppb U and 0.37ppb Th) [Ref Gerda paper]. The simulation shows a slightly larger tolerance for contaminated steel than for titanium, this is because SOURCES predicts a higher neutron mean energy in titanium. To our knowledge, no efforts to develop steel with contamination levels on the order of 10^{-4}ppb have been fructuous so steel vessels without internal shielding may not be a viable option for detectors of the size of CYGNUS. Regarding Titanium, the lowest concentrations reported in the LZ background assay [Ref LZ paper] are 7.29×10^{-3}ppb U and 5.66×10^{-2}ppb Th. These figures place the need for acrylic internal shielding slightly above 10cm. A steel vessel would require slightly more than 10cm of internal acrylic shielding, but given the small difference, the prohibitive cost of titanium may be an advantage to stainless steel vessels.

Finally, we turn our attention to designs based on acrylic vessel. This simulation can both test the viability of acrylic vessels and the effectiveness of the acrylic internal shield mentioned above. Indeed, the steel and titanium designs rely on the assumption that the contribution of the internal shield to the neutron flux would be negligible. The simulation of a 47 tonnes acrylic vessel shows a maximum concentration of $(6.607 \pm 0.004) \times 10^{-3}$pbb with a 1keV threshold and $(9.301 \pm 0.007) \times 10^{-3}$pbb with a 10keV threshold. These numbers are comparable to the radio-purity achieved in acrylic with SNO+, 2.35ppt ^{238}U and 9.60ppt ^{232}Th [ref SNO+ paper (Neil's email 21/10/16)].

Different vessel designs made of steel, titanium and acrylic have been compared. We showed that both steel and titanium, assuming the best concentrations of radio-nuclei available in the literature, require the addition of about 10cm of acrylic internal shielding in order to bring the nuclear recoil rate below one per year. In the case of a steel or titanium vessel, the additive contributions of the vessel and its inner shield to the neutron background would require that the concentrations of the different radio-nuclei be well below the maximum figures quoted in 4 and 5. We conclude that acrylic vessels are the preferred option in terms of managing the background levels.

Threshold	Concentration of 232-Th per gram (ppb/g)	Concentration of 238-U per gram (ppb/g)
1keV	$(9.35 \pm 0.02) \times 10^3$	$(1.870 \pm 0.004) \times 10^3$
10keV	$(1.182 \pm 0.003) \times 10^4$	$(2.363 \pm 0.005) \times 10^3$

Table 6: Maximum allowed concentrations of ^{238}U and ^{232}Th per grams of polymide in μ − PIC read-outs.

Threshold	Concentration of 232-Th and 238-U per gram (ppb/g)
1keV	$(5.6 \pm 0.1) \times 10^4$
10keV	$(7.3 \pm 0.2) \times 10^4$

Table 7: Maximum allowed concentrations of ^{238}U and ^{232}Th per grams of copper in GEMs read-out.

5.2.4. TPC read-out neutrons

Many of the current directional detectors [need ref to each one] have been built around different read-out technologies. In this section, we investigate the neutron background from the main materials used in each read-out. While backgrounds from the rock and the vessel are expected to dominate due to their relative size, the detector cannot be shielded from neutrons produced by the read-out materials. This and the large volume of CYGNUS make the careful selection of read-out materials an important part of the design process. In this section, we only explore the background level of the read-out, the comparison of their directional sensitivity is discussed in 5.6. For each material examined, we used SOURCES to estimate the neutron production rate for ^{238}U and ^{232}Th. We then simulated neutrons sampled from each spectra separately using Geant4 to obtain a separate figure for both decay chains. Similarly to the vessel background simulation, we fixed the U to Th ratio based on materials listed in [ref UKDM databank]. The simulated neutrons are produced in a sheet of the studied material placed inside the gas volume of the CYGNUS detector. The thickness of the sheet is chosen to resemble the typical thickness of the material simulated. For example, for the simulation of neutrons from ceramics, the thickness of the simulated sheet of ceramic was that of a resistor. From the results, we calculate the maximum concentration of ^{238}U and ^{232}Th per grams of material such that the neutron background from this material is less than 1 event per year with a threshold at either 1 or 10keV$_r$.

Firstly, we investigate the Micro Pixel Chamber (μ-PIC) readout as used in NEWAGE [ref NEWAGE + arXiv:hep-ex/0301012v2 for m uPICS]. The μ-PIC is constituted of a double sided circuit board separated by 100μm thick polymide substrate. The upper-limits on the concentrations of radioactive isotopes found by the NEWAGE collaboration are < 2.997ppb ^{238}U, < 6.642ppb ^{232}Th, and < 13.243ppm ^{40}K. 6 shows the results of the simulation for the $\mu-$PIC polymide. Based on an 0.8mm thick polymide and a drift distance of 50cm, the total mass of polymide can be estimate as roughly 2.2Ton corresponding to a maximum concentration on the order of 5.27×10^{-3}ppb for ^{232}Th and 1.05×10^{-3}ppb for ^{238}U.

The combination of pixel and Gas Electron Multipliers (GEMs) have been investigated as possible read-out for a TPC dark matter detector [Ref D3 arXiv:1110.3401 and UNM arXiv:1510.02170]. Thick GEMs are composed of two sheets of copper separated by ~0.4mm of kapton. Radio-pure copper can be manufactured with U and Th levels below 0.1ppb [Ref UKDM], but the concentration of these isotopes in kapton is about 8ppb ^{232}U and 9ppb ^{232}Th [Ref UKDM]. The results of the simulation are shown in 7 for copper and 8 for kapton. Assuming a 10μm thick copper coating on each GEM, we estimate the amount of copper for the whole detector to be around 179kg. The corresponding maximum concentration allowed is 0.32ppb for both U and Th with a 1keV threshold, and 0.41ppb with a 10keV threshold. We found these numbers to be acceptable as many copper samples measured in [REF UKDM] have contamination levels below these values. For kapton however, estimations based on 1.14Ton corresponding to a thickness of kapton of 0.4μm inside the GEMs, the maximum concentrations allowed are 2.27 (2.86)$\times 10^{-2}$ppb with a 1keV (10keV) threshold for both isotopes. These values are well below the current measured concentrations so a careful material selection will be necessary for this read-out.

A wire based read-out such as the one used in the DRIFT detector [REF arXiv:1701.00171] has two main sources of back-

Threshold	Concentration of 232-Th and 238-U per gram (ppb/g)
1keV	$(2.60 \pm 0.03) \times 10^4$
10keV	$(3.27 \pm 0.04) \times 10^4$

Table 8: Maximum allowed concentrations of ^{238}U and ^{232}Th per grams of kapton in GEMs read-out.

Threshold	Concentration of 232-Th per gram (ppb/g)	Concentration of 238-U per gram (ppb/g)
1keV	$(1.200 \pm 0.001) \times 10^4$	$(3.001 \pm 0.003) \times 10^3$
10keV	$(1.522 \pm 0.002) \times 10^4$	$(3.804 \pm 0.004) \times 10^3$

Table 9: Maximum allowed concentrations of ^{238}U and ^{232}Th per grams of ceramic in MWPCs read-out.

Threshold	Concentration of 232-Th per gram (ppb/g)	Concentration of 238-U per gram (ppb/g)
1keV	$(8.57 \pm 0.05) \times 10^4$	$(1.714 \pm 0.009) \times 10^5$
10keV	$(1.088 \pm 0.006) \times 10^5$	$(2.176 \pm 0.001) \times 10^5$

Table 10: Maximum allowed concentrations of ^{238}U and ^{232}Th per grams of steel in MWPCs read-out.

ground. Ceramics from resistors are known to have high U and Th concentrations, typically on the order of up to a few ppm. The amount of radio-isotopes can vary by a large amount depending on the batch, brand or type of resistors, so the future components of CYGNUS must be chosen carefully. The TREX-DM [ref arXiv:1601.01445] has tested several brands of high purity resistors and found that concentrations levels equivalent to 16ppb ^{238}U, < 2.80ppb ^{232}Th and 2.71ppm ^{40}K are achieveable . Furthermore, its is assumed that aluminium oxides are the main neutron emitters in resitors. Another potential source of neutrons is the steel making the wires of the MWPCs. The results for ceramics are summarized in 9, and the values for steel are shown in 10.

Using the DRIFT detector as an example, we estimated 1.94g of steel per meter cubed TPCs. This roughly corresponds to 3.9kg of steel for CYGNUS and the associated maximal contamination levels are 22.1(28)ppb for ^{232}Th with a 1(10)keV threshold and 44.2(56.1)ppb for ^{238}U with similar thresholds. This is well below the measured 5ppb ^{232}Th and 1.5ppb ^{238}U measured for the grid wires of the DRIFT-I vessel [ref UKDM]. Using again the DRIFT detector as an example, we estimated the quantity of ceramics as 22.6g per meter cubed TPCs [ref Carson], the corresponding maximum concentrations allowed for Cygnus are $5.31\,(6.73) \times 10^{-1}$ppb for ^{232}Th and $1.33\,(1.68) \times 10^{-1}$ppb for ^{238}U using the usual thresholds. These values are well below the 500ppb ^{238}U and 2000ppb ^{232}Th found in typical resistors.

In this section, we looked at the neutron background from (α, n) reactions and spontaneous fission from read-out materials used by the current direct detection experiments. While some materials met the background requirement of the CYGNUS detector, it seems no read-out technology is, in their current state, able the satisfy the CYGNUS background criteria. An important developmental step for CYGNUS will be to either perform extensive material screening in order to select only materials with the lowest amount of U and Th or to develop new ways to install the read out planes so as to minimise the amount of materials required.

5.2.5. Muon-induced neutrons and active vetoing

For the case of muon-induced neutrons, the muon energy spectrum and its angular distribution was simulated using the MUSUN simulation [ref Vitaly MUSUN paper]. MUSUN takes into account the angular profile and the composition of the rock overburden for the transportation of cosmic ray muons. The output is an array of the muon energies, positions and momenta. This array is inputted into the Geant4 simulation which simulates the final meters of the particles in the rock. The simulation allows for at least 20m of rock on each side of the detector to give each muon ample space to interact.

More than 200 million muons were simulated at the surface of the rock volume. A muon-veto was placed in the simulation outside of the external water shielding. The muon-vetos were represented as 1cm thick sheets of plastic scintillator placed on top of the detector and on each lateral sides. No muon-veto was placed below the detector. Muons entering these volumes are recorded in the simulation and latter used to veto nuclear recoils in the gas volume using coincidence of events. Similarly, the analysis searches for double nuclear scattering or electron recoils above the 1keV threshold recorded in the gas with a matching event number. There events are rejected as their are not WIMP candidate events. Using electron recoils as a way to veto nuclear recoils requires the simulation to be carried at nominal pressure. If this method is not used, the pressure can be increased but we found that in this configuration, the nuclear recoil rate is largely above 1/year. Since many muons are produced with energies on the TeV scale as seen in 7, we found that some events are recorded with recoil energies larger than what would be expected for a WIMP recoil. For this simulation, we explicitly limited the analysis to a region of interest situated between 1 and 100keV$_r$.

Muons passing the rock-cavern boundary are recorded in order to calculate the equivalent duration of the Monte-Carlo simulation. The number of muons recorded is compared to the measured value of the muon flux at the Boulby Underground Laboratory, $(4.09 \pm 0.15) \times 10^{-8}\text{cm}^{-2}/\text{s}^{-1}$, corresponding to a vertical rock overburden of 2805 ± 45m.w.e.. Using this technique,

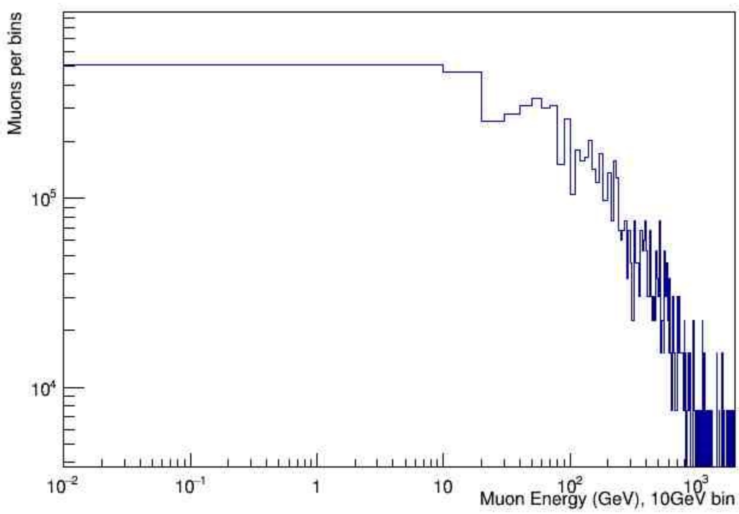

Figure 7: Muon energy spectrum at Boulby using MUSUN

we found that the simulation correspond to $(2.8 \pm 0.1) \times 10^7$s, during which no events were seen in the region of interest, leading to an upper-limit on the rate of muon-induced neutron nuclear recoil rate of 8.71×10^{-8}Hz.

5.2.6. Conclusion of neutron background

In the previous sections, we simulated the neutron background from the main sources. We saw that the external neutron background can easily be reduced by the use of a low-Z shielding material. For muon-induced neutrons, an excellent rejection rate can be achieved when combining an external muon veto and an analysis of coincidence between events in the gas. Many dark matter experiments have achieved a high muon-tagging efficiency with their muon veto, but the coincidence analysis ultimately depends on the capacity of the detector to be sensitive to Compton scattering and electron tracks while being able to contain the gamma background. This will be the subject of the next section. To palliate for a loss of efficiency in tagging muon induced events in the detector, PMTs could be installed in the water shield to increase the rejection capabilities of external events.

We reviewed the different materials available for the construction of a large vacuum vessel. Ultra-high purity stainless steel and titanium vessels with concentration of radio-nuclei < 100ppt but we found that considering the required mass the vessels, these concentrations are still not enough to be used without internal shielding. The SNO+ collaboration has achieved concentrations of radio-nuclei in acrylic about 10 time lower than the concentrations in the purest steel and titanium we considered during this study, making acrylic the current material of choice to build large dark matter TPC experiments.

We found that the choice of readout strategy greatly impacts on the internal neutron rate. Overall, no readout technology is currently standing out as the best option with regard to its neutron background. In each case, shown in 11 to 13, at least one material was producing too much neutron background. There may be several approach to this problem. Firstly, our simulation relies on an estimate of the quantity of each material inside a detector like CYGNUS. It may be possible to either reduce the required quantity of problematic materials through careful design and planning. Alternative materials may be investigated or higher purity versions of the same materials may be developed. This is particularly relevant to the $\mu-$pic and GEMs options for which better refined glass polymids are being developed and GEMs with high purity G10 insulator instead of kapton are being investigated. [can I say by some of the authors, to account for the different CYGNUS R&D projects ?] In the case of ceramics for the wire readout strategy, it may also be possible to shield the pre-amplifier, or eventually move them outside of the vessel in order to further reduce the neutron background.

5.3. Gamma Backgrounds

In the previous section, we showed that the neutron background can be mitigated by the careful selection of radio-pure materials. The associated gamma background required different shielding technique. For example, the detector can be shielded from

Material	Neutron background $\left(\text{year}^{-1}\right)$	Gamma background $\left(\text{year}^{-1}\right)$
Rock	< 0.93 (90%CL)	$(2.82 \pm 0.04) \times 10^{10}$
Vessel (acrylic)	0.138 ± 0.001	$(2.805 \pm 0.002) \times 10^{7}$
Glass Polymid	$< 64.5 \pm 0.3$	$< (1.3586 \pm 0.0003) \times 10^{8}$

Table 11: Neutron and Gamma background for μ − pics readout between 1 − 100keV

Material	Neutron background $\left(\text{year}^{-1}\right)$	Gamma background $\left(\text{year}^{-1}\right)$
Rock	< 0.93 (90%CL)	$(2.82 \pm 0.04) \times 10^{10}$
Vessel (acrylic)	0.138 ± 0.001	$(2.805 \pm 0.002) \times 10^{7}$
Copper	$< 1.036 + 0.005$	$(4.702 \pm 0.002) \times 10^{7}$
Kapton	22.4 ± 0.1	$(2.515 \pm 0.001) \times 10^{8}$

Table 12: Neutron and Gamma background for GEMs readout between 1 − 100keV

the gamma background originating from the rock by building a Lead castle. However, this new element would also contribute to the neutron background. TPCs can be made insensitive to their gamma background as demonstrated in [Ref arXiv:1701.00171] by raising the threshold such that the smaller $^{dE}/_{dx}$ for electron tracks does not trigger the analysis. This technique can be used for CYGNUS at the cost of efficiency and sensitivity to low mass WIMP recoils. Another technique is to use the full 3 − D potential of certain readouts such as CCD cameras. This approach, developed in [Ref arXiv:1703.09883 and arXiv:1510.02170], relies on the low threshold of the CCD cameras to veto electron tracks based on the different shape of the Bragg curves for example. The problem with this techniques lies again in the balance between the rate of neutron and gamma backgrounds. We found that pixelated readouts contain a large amounts of heavy metals and other components with a typically large concentration of ^{238}U and ^{232}Th.

In this section, we report on the simulation of the gamma background in the different materials relevant to CYGNUS. Using Geant4, we homogeneously populated the rock, vessel, and sheets of readout materials with ^{238}U,^{232} Th and ^{40}K at rest. Geant4 will automatically simulate the decay chains of the different isotopes with the correct branching ratio. For materials with relatively small thicknesses, such as the vessel or readouts, the homogeneous distribution of the isotopes allows for the simultaneous simulation of bulk and surface background. In the case of the rock, a simulation similar to the one described in 5 showed that only the first 30cm of rock contributes to the gamma background. Beyond this distance, the self-shielding capabilities of the rock are sufficient to stop radiation from leaking.

5.4. Radon and Radon Progeny Backgrounds

Radon gas emanating from materials is a major source background for rare events experiments. In particular, the low energy (∼ 100keV) of radon progeny recoils (RPRs) can mimic a WIMP interaction. ^{222}Rn being a noble gas, its low chemical reactivity makes it particularly difficult to deal with. Moreover, its 3.8 day half-life allows it to spread from the materials where it is produced, making radon a widespread source of background. α-decays of gaseous radon inside the fiducial volume can easily be identified if the associated alpha particle is fully contained. RPRs occurring in the bulk or surface of materials may prove harder to reject. In this case, the associated alpha particle may not be detected, if for example it remains trapped inside the materials. For these surface events, it is possible for a daughter nuclear recoil to enter the amplification region and be recorded as a signal, if the associated alpha particle is not detected, this event constitute a background to the dark matter search. Many efforts from

Material	Neutron background $\left(\text{year}^{-1}\right)$	Gamma background $\left(\text{year}^{-1}\right)$
Rock	< 0.93 (90%CL)	$(2.82 \pm 0.04) \times 10^{10}$
Vessel (acrylic)	0.138 ± 0.001	$(2.805 \pm 0.002) \times 10^{7}$
Steel wires	$(2.26 \pm 0.01) \times 10^{-2}$	$(7.583 \pm 0.003) \times 10^{4}$
Ceramics	3.02 ± 0.01	$< (2.24 \pm 0.01) \times 10^{6}$

Table 13: Neutron and Gamma background for MWPCs readout between 1 − 100keV

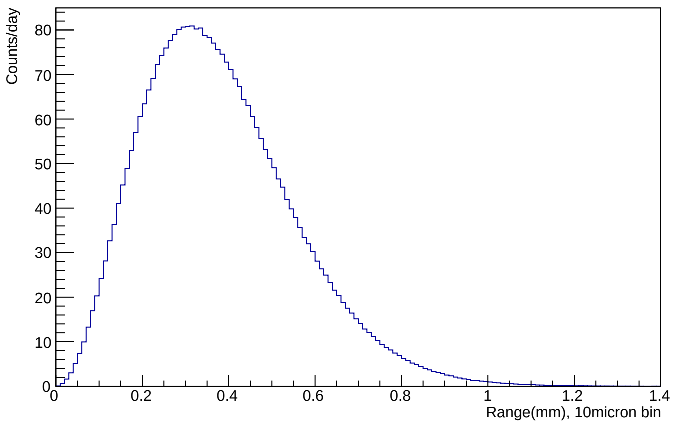

Figure 8: Simulated range of RPRs in 50Torr of SF_6

directional detectors have been directed to study and control radon background. In particular, an important mitigation effort was done by the DRIFT collaboration [ref Steve paper on radon arXiv 1407.3938, can include E. Miller cathode paper] to measure and limit radon emanation in the detector. The MIMAC group [ref 1504.05865] also has demonstrated successful detection of radon events. An analysis cut based on the z-position of the events was used to reject RPRs originating from the anode and cathode, where RPRs are an important background due to the high U and Th concentration of Micromegas PCBs.

If the detector is composed of back to back TPCs, cathode-crosser events are unambiguous traces of radon and can be vetoed based on the time coincidence of the charge deposition in both sides of the detector. These events can be used to estimate the level of radon present in the detector as done in [same papers DRIFT + MIMAC]. In DRIFT, these events are vetoed by reducing the fiducial region such that any events detected less than 2cm away from the cathode are rejected [Ref ArXiv1701.00171]. The size of this region is affected by the diffusion of the minority peaks which lowers their amplitudes and hinders the z-reconstruction capabilities of the detector. Furthermore, the precision of the extrapolation of a z position also depends on the time separation of the minority peaks [ref DPSI arXiv1308.0354], better results are obtained when using the P-peak due to its larger separation with the main peak. In this case, the z-resolution is 0.33cm.

Using Geant4, we simulated the range of ^{222}Rn decays and RPRs in CYGNUS. Considering that ^{220}Rn in negligible compared to ^{222}Rn, we simulated a fixed source of ^{222}Rn placed inside the fiducial volume of detector filled with 50Torr of SF_6 as in the previous simulations. Since we are only interested in the range of the nuclear recoils, there is no need to populate the gas homogeneously with ^{222}Rn and the same information can be deduced from a fixed source simulation. Secular equilibrium is assumed throughout the decay chain. The purpose of this simulation is to test the validity of a cut placed 2cm away from the cathode to reject cathode RPRs as described above for the DRIFT detector. The cathode RPR rate we used for CYGNUS is inferred by the rate observed in DRIFT as 3.4 ± 0.4events/day/m^{2}of cathode. 8 shows the full range of the events recorded in the simulation. The z resolution function measured in [ref DPSI arXiv1308.0354] is then applied to the simulated recoil range by adding a random number sampled from a Gaussian distribution with mean 0 and variance 0.33cm to the simulated z-range. Finally, by integrating the smeared distribution of z-ranges, the estimated RPRs rate with a z-range above 2cm can be estimated at 2.57×10^{-16}events/day (90%CL).

While these results would justify the position of the cut at 2cm, many of the parameters used were borrowed from the DRIFT detector. If the existence of minority carriers in SF_6 is proven to be usable, the different resolution of the minority peaks will most likely provide different results.

5.5. Surface and other Backgrounds

5.6. Comparison of Technologies for low background

6. Underground Sites and Engineering

[Section organizer: Neil Spooner]

This section provides a summary of the more significant issues regarding underground site requirements for directional dark matter detectors and associated engineering requirements. In the event that a solid state solution for directionality proves viable then there are no particular issues that are different from those addressed by the non-directional community, except in the case of emulsion technology. For the latter, because this concept does not provide real time data, there is need to provide continuous rotation and pointing of the instrument to maintain a fixed orientation in galactic coordinates. Depending on the intrinsic backgrounds achievable the moving part may need to include all or some of the shielding and the extra mass that this would entail, as well as the detector itself. Given the need to allow space for the mechanism of sufficient power to drive the movement this could have an impact on the space requirements in a laboratory. However, quantifying this challenge will need to wait until there is more information on the emulsion technique and its feasibility for directional detection with large target mass.

More is known about the implications for site installation imposed by the low pressure gas TPC technologies. Here the main challenge is the potential space requirement of the experiment but also the need to provide handling of the gas target underground. Both these factors depend on the choice of gas and operating pressure. Regarding engineering of the detector vessel itself this is driven by three main issues: (i) the requirement that it likely will need to be a vacuum vessel, (ii) the need to use materials with low intrinsic background, specifically so that the neutron rate is below the required specification, typically seen as <1 neutron induced event per year, and (iii) any restrictions on site access that may impose a limit in the size of individual components taken underground. A further consideration is the requirement on site overburden. However, for the sites currently under consideration for CYGNUS, all >1km in depth, this is not found to be a major issue. At this depth, as shown in sec X, although there is a significant potential number of muon induced neutron events, these can be rejected by a combination of an active external muon veto and by making use of the powerful EM detection capabilities of the TPC technology. The need for an external veto could have a modest impact on the overall dimensions of the experiment, depending on the gas readout technology adopted and its discrimination power. In the worst case scenario of a full 4pi veto with maximum efficiency the extra linear space required, assuming a conventional plastic scintillator veto, would be < 1m.

The first stage experiment for a CYGNUS TPC is considered to be one that can reach the neutrino floor around the solar neutrino "knee area", at recoil energies around 10-20 keV. This requires a vessel of order 10 m3 volume plus external low-Z neutron, plus some degree of gamma shielding (depending on the rejection capability of the readout chosen), together adding up to ~1m. At the required sensitivity, assuming < 1 background neutron per year, it is feasible to obtain steel of sufficient radio-purity that recourse to more complex, lower background designs, for instance using acrylic, would not be needed. The scale and engineering requirements are therefore unlikely to be challenging for any of the possible underground sites although constraints on the maximum size of object able to enter some of the sites, e.g. 2 x 2m at Boulby, would need to be allowed for in the vessel design. Fig. x shows a typical design for 10 m3 CYGNUS vessel based on steel construction. This simple cubic shape vacuum vessel with hinged door access follows the successful design adopted for the DRIFT-II detectors [ref] though with the door hinges pivoting to provide extra strength. A variety of designs for external neutron and gamma shielding are possible. Use of interlocking plastic water containers is one possibility, as adopted for the DRIFT upgrade shielding, see Fig 2a, An alternative design is to use a purpose built water containing, see Fig. 2b, which is more expensive but has the potential advantage that it could be instrumented with photomultipliers to provide a Cherenkov muon veto.

An advantage of the gas TPC concept is that there is no particular restriction on the shape of the experiment. For instance, an elongated "worm-like" sectional design, where one dimension is substantially longer than the other two, is feasible, and actually has certain advantages for operations and maintenance. This feature makes CYGNUS well suited to sites where long tunnels and restrictions on available height are normal, such as mine sites like Stawell or Boulby. The relative simplicity of the services needed, in particular that there are no cryogenics involved, also is an advantage here. Additionally, as sated in sec 1. the experiment can be built as separate detectors, either in one site, or in multiple sites. This also allows advantage to be taken of cross-correlating data at different latitudes so as to aid control of systematics.

The geometric features above are not necessarily required for a first 10 m3 stage but could become important in designs aiming to achieve full directional signals below the neutrino floor, typically 1000 m3. A baseline geometry of a single 10 x 10 x 10m vessel has been studied here. Such a vessel could be engineered in sites such as LNGS, where there is available head-room and good access, though the same principles would apply to a segmented detector of the same total volume distributed in different sites, or an elongated version of say 5 x 5 x 40m that would conceivably fit in an existing facility at Boulby.

The next engineering constraint on the vessel at this scale comes from the need to maintain essentially zero neutron background and hence U/Th radio-purity in the vessel at a level x100 better than for the 10 m3 version. This rules out an all-steel design, assuming no progress can be made towards higher purity steel than the best currently obtainable. A natural alternative low background construction material is acrylic. This has been successfully used by the DEEP and SNO collaborations to construct their substantial detector vessels. They have also proven that ultra-low backgrounds can be achieved in acrylic (< x ppt)[ref], sufficiently low to meet the requirements for CYGNUS. The use of an acrylic vacuum vessel for a low pressure TPC has also been successfully demonstrated by the UNM group [ref], where a cylindrical design was adopted, as shown in Fig. 3. This concept, in which also the field rings where applied directly to the inner surface of the vacuum vessel, was shown to have significant advantage over the conventional concept whereby a separate field cage is needed, mounted away from the inner surface of a steel vessel, as in DRIFT-II and others. For instance, the design minimises the presence of sharp edges and in their case allowed higher drift and cathode voltages to be applied before breakdown.

Nevertheless, the constraint required for CYGNUS that the vessel be capable of withstanding a vacuum adds significant challenges for an all-acrylic version at the 1000m3 scale. Acrylic is substantially less strong than steel and so that although a large cylindrical vessel can be considered an option, the preferred modular cubic design currently looks ruled out for practical purposes in acrylic, even when combined with high thickness acrylic support bars. Hence, for now three alternative solutions have been studied. The first of these is to revert to an all steel design, using the best purity steel and with the total mass minimised, but with the addition of an internal neutron passive shield comprising acrylic sheet fixed to the inside of the walls. The GEANT4 simulations detailed in sec. x have shown that of order 10cm thickness only would be needed. A second option is to consider a hybrid design in which acrylic is used to replace the main vessel panels but steel retained for the main support structures. Fig. x shows an example concept for this by the Melbourne group. A factor of 10-20 reduction in background can be achieved. Combining this with some internal neutron shielding and/or more stringent selection of steel could achieve the goal. Thirdly, it may be possible to run at 1 atm pressure by using He as a filler gas. If it can be additionally proven that flushing gas through the vessel prior to operation can provide sufficient purification of contaminants, rather than the conventional use of outgassing under vacuum, then this would obviate the need for the vessel to be of vacuum standard, greatly reducing the mass of steel or acrylic needed. This option is under investigation, noting that negative ion gases, namely CS2 and SF6 are already known to be highly tolerant of impurity gases. For instance DRIFT operates well with up to 1% impurity gases.

Whilst there is no need for complex cryogenics engineering in CYGNUS consideration is needed of the engineering aspects of the gas supply. In the current generation of detectors the target gas is generally flowed and disposed of through filters to the atmosphere. However, for CYGNUS re-circulation will be needed, both for cost and environmental reasons, particularly for SF6 which is a powerful greenhouse gas. Recirculation also provides a potential means for reduction of radon from the target. Purification of SF6 is well known in industry and so not seen as a major issue here. Meanwhile, recent experiments by the Sheffield group have now shown for the first time that active radon removal in SF6 is also possible. Fig. x shows results of an experiment in which SF6 was circulated through a vessel with a known level of radon added via a sealed radon surce. When the gas is diverted through a molecular sieve the radon is seen to reduce (green points on Fig. x). When this filter is cooled with dry ice (blue points) a further reduction is seen. In this experiment an earlier test was performed to check that the SF6 was not itself absorbed by the filter.

Summarising this brief overview of CYGNUS engineering we conclude that while the required vessels do present an engineering challenge these should be surmountable. There is also significant flexibility in the approach to the shape and modularisation plus prospect for construction in sections underground and at multiple sites, meaning constraints imposed by all the proposed sites can be met. Finally, it is worth noting that the baseline 10 x 10 x 10 m vessel represents less than 1/20th of the cryogenic vessel proposed for the DUNE experiment at Sandford Underground laboratory for which rock excavation is now underway.

7. Conceptual Design Strategy

[Section organizer: all]

This summarizes the above technology discussions and briefly outlines possible scenarios and a straw man design for a Galactic Recoil Observatory

8. Conclusion

[Section organizer: all]

This section restates the science case in light of the technology discussion and provides comment on the likely feasibility, cost and design of a future large scale galactic recoil observatory.

References

[1] T. Kim, M. Freytsis, J. Button-Shafer, J. Kadyk, S. Vahsen, W. Wenzel, Readout of TPC tracking chambers with GEMs and pixel chip, Nucl. Instrum. MethodsA589 (2008) 173–184. doi:10.1016/j.nima.2008.02.049.

[2] T. MarrodÃąn Undagoitia, L. Rauch, Dark matter direct-detection experiments, J. Phys. G43 (1) (2016) 013001. arXiv:1509.08767, doi:10.1088/0954-3899/43/1/013001.

[3] R. Bernabei, et al., Final model independent result of DAMA/LIBRA-phase1, Eur. Phys. J. C73 (2013) 2648. arXiv:1308.5109, doi:10.1140/epjc/s10052-013-2648-7.

[4] J. AmarÃl', et al., From ANAIS-25 towards ANAIS-250, Phys. Procedia 61 (2015) 157–162. arXiv:1404.3564, doi:10.1016/j.phpro.2014.12.026.

[5] E. Shields, J. Xu, F. Calaprice, SABRE: A New NaI(T1) Dark Matter Direct Detection Experiment, Phys. Procedia 61 (2015) 169–178. doi:10.1016/j.phpro.2014.12.028.

[6] G. Adhikari, et al., Design and Initial Performance of the COSINE-100 ExperimentarXiv:1710.05299.

[7] D. N. Spergel, The motion of the Earth and the detection of WIMPs, Phys. Rev.D37 (1988) 1353. doi:10.1103/PhysRevD.37.1353.

[8] J. Billard, F. Mayet, D. Santos, Assessing the discovery potential of directional detection of Dark Matter, Phys. Rev.D85 (2012) 035006. arXiv:1110.6079, doi:10.1103/PhysRevD.85.035006.

[9] P. Grothaus, M. Fairbairn, J. Monroe, Directional Dark Matter Detection Beyond the Neutrino Bound, Phys. Rev.D90 (5) (2014) 055018. arXiv:1406.5047, doi:10.1103/PhysRevD.90.055018.

[10] C. A. J. O'Hare, A. M. Green, J. Billard, E. Figueroa-Feliciano, L. E. Strigari, Readout strategies for directional dark matter detection beyond the neutrino background, Phys. Rev.D92 (6) (2015) 063518. arXiv:1505.08061, doi:10.1103/PhysRevD.92.063518.

[11] S. K. Lee, A. H. G. Peter, Probing the Local Velocity Distribution of WIMP Dark Matter with Directional Detectors, J. Cosmol. Astropart. Phys.1204 (2012) 029. arXiv:1202.5035, doi:10.1088/1475-7516/2012/04/029.

[12] J. B. R. Battat, et al., Radon in the DRIFT-II directional dark matter TPC: emanation, detection and mitigation, J. Instrum.9 (11) (2014) P11004. arXiv:1407.3938, doi:10.1088/1748-0221/9/11/P11004.

[13] D. Santos, J. Billard, G. Bosson, J. Bouly, O. Bourrion, et al., MIMAC : A micro-tpc matrix for directional detection of dark matter, EAS Publ. Ser.53 (2012) 25–31. arXiv:1111.1566, doi:10.1051/eas/1253004.

[14] C. Deaconu, Recent progress from the DMTPC directional dark matter experiment, in: UCLA 11th Symposium on Sources and Detection of Dark Matter and Dark Energy in the Universe, 2014.

[15] K. Miuchi, et al., First underground results with NEWAGE-0.3a direction-sensitive dark matter detector, Phys. Lett. B686 (2010) 11–17. arXiv:1002.1794, doi:10.1016/j.physletb.2010.02.028.

[16] G. Angloher, et al., Results on light dark matter particles with a low-threshold CRESST-II detector, Eur. Phys. J. C76 (1) (2016) 25. arXiv:1509.01515, doi:10.1140/epjc/s10052-016-3877-3.

[17] R. Agnese, et al., Low-Mass Dark Matter Search with CDMSlite, Submitted to: Phys. Rev. DarXiv:1707.01632.

[18] L. Hehn, et al., Improved EDELWEISS-III sensitivity for low-mass WIMPs using a profile likelihood approach, Eur. Phys. J. C76 (10) (2016) 548. arXiv:1607.03367, doi:10.1140/epjc/s10052-016-4388-y.

[19] C. Amole, et al., Dark Matter Search Results from the PICO-2L C_3F_8 Bubble Chamber, Phys. Rev. Lett. 114 (23) (2015) 231302. arXiv:1503.00008, doi:10.1103/PhysRevLett.114.231302.

[20] C. Amole, et al., Dark matter search results from the PICO-60 CF_3I bubble chamber, Phys. Rev. D93 (5) (2016) 052014. arXiv:1510.07754, doi:10.1103/PhysRevD.93.052014.

[21] P. Agnes, et al., Results from the first use of low radioactivity argon in a dark matter search, Phys. Rev. D93 (8) (2016) 081101. arXiv:1510.00702, doi:10.1103/PhysRevD.93.081101.

[22] A. Tan, et al., Dark Matter Results from First 98.7 Days of Data from the PandaX-II Experiment, Phys. Rev. Lett. 117 (12) (2016) 121303. arXiv:1607.07400, doi:10.1103/PhysRevLett.117.121303.

[23] D. S. Akerib, et al., Results from a search for dark matter in the complete LUX exposure, Phys. Rev. Lett. 118 (2) (2017) 021303. arXiv:1608.07648, doi:10.1103/PhysRevLett.118.021303.

[24] E. Aprile, et al., First Dark Matter Search Results from the XENON1T ExperimentarXiv:1705.06655.

[25] R. Agnese, et al., Projected Sensitivity of the SuperCDMS SNOLAB experiment, Phys. Rev. D95 (8) (2017) 082002. arXiv:1610.00006, doi:10.1103/PhysRevD.95.082002.

[26] D. S. Akerib, et al., LUX-ZEPLIN (LZ) Conceptual Design ReportarXiv:1509.02910.

[27] J. Aalbers, et al., DARWIN: towards the ultimate dark matter detector, JCAP 1611 (2016) 017. arXiv:1606.07001, doi:10.1088/1475-7516/2016/11/017.

[28] C. E. Aalseth, et al., Maximum Likelihood Signal Extraction Method Applied to 3.4 years of CoGeNT DataarXiv:1401.6234.

[29] P. Gondolo, Recoil momentum spectrum in directional dark matter detectors, Phys. Rev. D66 (2002) 103513. arXiv:hep-ph/0209110, doi:10.1103/PhysRevD.66.103513.

[30] A. M. Green, B. Morgan, The median recoil direction as a WIMP directional detection signal, Phys. Rev.D81 (2010) 061301. arXiv:1002.2717, doi:10.1103/PhysRevD.81.061301.

[31] J. Billard, F. Mayet, J. F. Macias-Perez, D. Santos, Directional detection as a strategy to discover galactic Dark Matter, Phys. Lett.B691 (2010) 156–162. arXiv:0911.4086, doi:10.1016/j.physletb.2010.06.024.

[32] N. Bozorgnia, G. B. Gelmini, P. Gondolo, Ring-like features in directional dark matter detection, J. Cosmol. Astropart. Phys.1206 (2012) 037. arXiv:1111.6361, doi:10.1088/1475-7516/2012/06/037.

[33] N. Bozorgnia, G. B. Gelmini, P. Gondolo, Aberration features in directional dark matter detection, J. Cosmol. Astropart. Phys.1208 (2012) 011. arXiv:1205.2333, doi:10.1088/1475-7516/2012/08/011.

[34] B. Cabrera, L. M. Krauss, F. Wilczek, Bolometric Detection of Neutrinos, Phys. Rev. Lett. 55 (1985) 25. doi:10.1103/PhysRevLett.55.25.

[35] J. Monroe, P. Fisher, Neutrino Backgrounds to Dark Matter Searches, Phys. Rev. D76 (2007) 033007. arXiv:0706.3019, doi:10.1103/PhysRevD.76.033007.

[36] L. E. Strigari, Neutrino Coherent Scattering Rates at Direct Dark Matter Detectors, New J. Phys. 11 (2009) 105011. arXiv:0903.3630, doi:10.1088/1367-2630/11/10/105011.
[37] A. Gutlein, et al., Solar and atmospheric neutrinos: Background sources for the direct dark matter search, Astropart. Phys. 34 (2010) 90–96. arXiv:1003.5530, doi:10.1016/j.astropartphys.2010.06.002.
[38] J. Billard, L. Strigari, E. Figueroa-Feliciano, Implication of neutrino backgrounds on the reach of next generation dark matter direct detection experiments, Phys. Rev.D89 (2) (2014) 023524. arXiv:1307.5458, doi:10.1103/PhysRevD.89.023524.
[39] J. F. Beacom, The Diffuse Supernova Neutrino Background, Ann. Rev. Nucl. Part. Sci. 60 (2010) 439–462. arXiv:1004.3311, doi:10.1146/annurev.nucl.010909.083331.
[40] G. Battistoni, A. Ferrari, T. Montaruli, P. R. Sala, The atmospheric neutrino flux below 100-MeV: The FLUKA results, Astropart. Phys. 23 (2005) 526–534. doi:10.1016/j.astropartphys.2005.03.006.
[41] M. Honda, T. Kajita, K. Kasahara, S. Midorikawa, Improvement of low energy atmospheric neutrino flux calculation using the JAM nuclear interaction model, Phys. Rev. D83 (2011) 123001. arXiv:1102.2688, doi:10.1103/PhysRevD.83.123001.
[42] F. Ruppin, J. Billard, E. Figueroa-Feliciano, L. Strigari, Complementarity of dark matter detectors in light of the neutrino background, Phys. Rev.D90 (8) (2014) 083510. arXiv:1408.3581, doi:10.1103/PhysRevD.90.083510.
[43] J. B. Dent, B. Dutta, J. L. Newstead, L. E. Strigari, Effective field theory treatment of the neutrino background in direct dark matter detection experiments, Phys. Rev. D93 (7) (2016) 075018. arXiv:1602.05300, doi:10.1103/PhysRevD.93.075018.
[44] J. B. Dent, B. Dutta, J. L. Newstead, L. E. Strigari, Dark matter, light mediators, and the neutrino floor, Phys. Rev. D95 (5) (2017) 051701. arXiv:1607.01468, doi:10.1103/PhysRevD.95.051701.
[45] C. A. O'Hare, Dark matter astrophysical uncertainties and the neutrino floor, Phys. Rev. D94 (6) (2016) 063527. arXiv:1604.03858, doi:10.1103/PhysRevD.94.063527.
[46] J. H. Davis, Dark Matter vs. Neutrinos: The effect of astrophysical uncertainties and timing information on the neutrino floor, JCAP 1503 (2015) 012. arXiv:1412.1475, doi:10.1088/1475-7516/2015/03/012.
[47] N. Agafonova, et al., Discovery potential for directional Dark Matter detection with nuclear emulsionsarXiv:1705.00613.
[48] T. Franarin, M. Fairbairn, Reducing the solar neutrino background in dark matter searches using polarized helium-3, Phys. Rev. D94 (5) (2016) 053004. arXiv:1605.08727, doi:10.1103/PhysRevD.94.053004.
[49] G. Battistoni, A. Ferrari, T. Montaruli, P. R. Sala, The FLUKA atmospheric neutrino flux calculation, Astropart. Phys. 19 (2003) 269–290, [Erratum: Astropart. Phys.19,291(2003)]. arXiv:hep-ph/0207035, doi:10.1016/S0927-6505(02)00246-3.
[50] J. Bovy, S. Tremaine, On the local dark matter density, Astrophys. J. 756 (2012) 89. arXiv:1205.4033, doi:10.1088/0004-637X/756/1/89.
[51] J. I. Read, The Local Dark Matter Density, J. Phys. G41 (2014) 063101. arXiv:1404.1938, doi:10.1088/0954-3899/41/6/063101.
[52] M. Vogelsberger, A. Helmi, V. Springel, S. D. M. White, J. Wang, C. S. Frenk, A. Jenkins, A. D. Ludlow, J. F. Navarro, Phase-space structure in the local dark matter distribution and its signature in direct detection experiments, Mon. Not. Roy. Astron. Soc. 395 (2009) 797–811. arXiv:0812.0362, doi:10.1111/j.1365-2966.2009.14630.x.
[53] J. D. Sloane, M. R. Buckley, A. M. Brooks, F. Governato, Assessing Astrophysical Uncertainties in Direct Detection with Galaxy Simulations, Astrophys. J. 831 (2016) 93. arXiv:1601.05402, doi:10.3847/0004-637X/831/1/93.
[54] M. J. Reid, et al., Trigonometric Parallaxes of High Mass Star Forming Regions: the Structure and Kinematics of the Milky Way, Astrophys. J. 783 (2014) 130. arXiv:1401.5377, doi:10.1088/0004-637X/783/2/130.
[55] A. H. G. Peter, WIMP astronomy and particle physics with liquid-noble and cryogenic direct-detection experiments, Phys. Rev. D83 (2011) 125029. arXiv:1103.5145, doi:10.1103/PhysRevD.83.125029.
[56] B. J. Kavanagh, A. M. Green, Model independent determination of the dark matter mass from direct detection experiments, Phys. Rev. Lett. 111 (3) (2013) 031302. arXiv:1303.6868, doi:10.1103/PhysRevLett.111.031302.
[57] C. McCabe, The Astrophysical Uncertainties Of Dark Matter Direct Detection Experiments, Phys. Rev. D82 (2010) 023530. arXiv:1005.0579, doi:10.1103/PhysRevD.82.023530.
[58] B. J. Kavanagh, Discretising the velocity distribution for directional dark matter experiments, JCAP 1507 (07) (2015) 019. arXiv:1502.04224, doi:10.1088/1475-7516/2015/07/019.
[59] B. J. Kavanagh, C. A. J. O'Hare, Reconstructing the three-dimensional local dark matter velocity distribution, Phys. Rev. D94 (12) (2016) 123009. arXiv:1609.08630, doi:10.1103/PhysRevD.94.123009.
[60] C. A. J. O'Hare, A. M. Green, Directional detection of dark matter streams, Phys. Rev. D90 (12) (2014) 123511. arXiv:1410.2749, doi:10.1103/PhysRevD.90.123511.
[61] C. W. Purcell, A. R. Zentner, M.-Y. Wang, Dark Matter Direct Search Rates in Simulations of the Milky Way and Sagittarius Stream, JCAP 1208 (2012) 027. arXiv:1203.6617, doi:10.1088/1475-7516/2012/08/027.
[62] M. Kuhlen, M. Lisanti, D. N. Spergel, Direct Detection of Dark Matter Debris Flows, Phys. Rev. D86 (2012) 063505. arXiv:1202.0007, doi:10.1103/PhysRevD.86.063505.
[63] K. I. Nagao, R. Yakabe, T. Naka, K. Miuchi, Discrimination of anisotropy in dark matter velocity distribution with directional detectorsarXiv:1707.05523.
[64] D. Tucker-Smith, N. Weiner, Inelastic dark matter, Phys. Rev.D64 (2001) 043502. arXiv:hep-ph/0101138, doi:10.1103/PhysRevD.64.043502.
[65] D. P. Finkbeiner, T. Lin, N. Weiner, Inelastic Dark Matter and DAMA/LIBRA: An Experimentum Crucis, Phys. Rev. D80 (2009) 115008. arXiv:0906.0002, doi:10.1103/PhysRevD.80.115008.
[66] M. Lisanti, J. G. Wacker, Disentangling Dark Matter Dynamics with Directional Detection, Phys. Rev. D81 (2010) 096005. arXiv:0911.1997, doi:10.1103/PhysRevD.81.096005.
[67] R. Laha, Directional detection of dark matter in universal bound states, Phys. Rev. D92 (2015) 083509. arXiv:1505.02772, doi:10.1103/PhysRevD.92.083509.
[68] J. Fan, M. Reece, L.-T. Wang, Non-relativistic effective theory of dark matter direct detection, JCAP 1011 (2010) 042. arXiv:1008.1591, doi:10.1088/1475-7516/2010/11/042.
[69] B. J. Kavanagh, New directional signatures from the nonrelativistic effective field theory of dark matter, Phys. Rev. D92 (2) (2015) 023513. arXiv:1505.07406, doi:10.1103/PhysRevD.92.023513.

[70] R. Catena, Dark matter directional detection in non-relativistic effective theories, JCAP 1507 (07) (2015) 026. arXiv:1505.06441, doi:10.1088/1475-7516/2015/07/026.
[71] R. D. Peccei, H. R. Quinn, CP conservation in the Presence of Instantons, Phys. Rev. Lett.38 (1977) 1440–1443. doi:10.1103/PhysRevLett.38.1440.
[72] J. E. Kim, G. Carosi, Axions and the Strong CP Problem, Rev. Mod. Phys. 82 (2010) 557–602. arXiv:0807.3125, doi:10.1103/RevModPhys.82.557.
[73] A. Arvanitaki, S. Dimopoulos, S. Dubovsky, N. Kaloper, J. March-Russell, String Axiverse, Phys. Rev.D81 (2010) 123530. arXiv:0905.4720, doi:10.1103/PhysRevD.81.123530.
[74] L. F. Abbott, P. Sikivie, A Cosmological Bound on the Invisible Axion, Phys. Lett. B120 (1983) 133–136. doi:10.1016/0370-2693(83)90638-X.
[75] M. Dine, W. Fischler, The Not So Harmless Axion, Phys. Lett. B120 (1983) 137–141. doi:10.1016/0370-2693(83)90639-1.
[76] J. Preskill, M. B. Wise, F. Wilczek, Cosmology of the Invisible Axion, Phys. Lett. B120 (1983) 127–132. doi:10.1016/0370-2693(83)90637-8.
[77] S. Chang, C. Hagmann, P. Sikivie, Studies of the motion and decay of axion walls bounded by strings, Phys. Rev. D59 (1999) 023505. arXiv:hep-ph/9807374, doi:10.1103/PhysRevD.59.023505.
[78] M. Kawasaki, K. Saikawa, T. Sekiguchi, Axion dark matter from topological defects, Phys. Rev. D91 (6) (2015) 065014. arXiv:1412.0789, doi:10.1103/PhysRevD.91.065014.
[79] A. R. Liddle, M. S. Madsen, The Structure and formation of boson stars, Int. J. Mod. Phys. D1 (1992) 101–144. doi:10.1142/S0218271892000057.
[80] C. J. Hogan, M. J. Rees, AXION MINICLUSTERS, Phys. Lett. B205 (1988) 228–230. doi:10.1016/0370-2693(88)91655-3.
[81] E. W. Kolb, I. I. Tkachev, Large amplitude isothermal fluctuations and high density dark matter clumps, Phys. Rev. D50 (1994) 769–773. arXiv:astro-ph/9403011, doi:10.1103/PhysRevD.50.769.
[82] D. J. E. Marsh, Axion Cosmology, Phys. Rept. 643 (2016) 1–79. arXiv:1510.07633, doi:10.1016/j.physrep.2016.06.005.
[83] P. W. Graham, S. Rajendran, New Observables for Direct Detection of Axion Dark Matter, Phys. Rev. D88 (2013) 035023. arXiv:1306.6088, doi:10.1103/PhysRevD.88.035023.
[84] D. S. Akerib, et al., First searches for axions and axion-like particles with the LUX experimentarXiv:1704.02297.
[85] E. Aprile, et al., First Axion Results from the XENON100 Experiment, Phys. Rev. D90 (6) (2014) 062009. arXiv:1404.1455, doi:10.1103/PhysRevD.90.062009.
[86] C. Fu, et al., Limits on Axion Couplings from the First 79.8-Day Data of the PandaX-II ExperimentarXiv:1707.07921.
[87] A. Derbin, I. Drachnev, A. Kayunov, V. Muratova, Search for solar axions produced by Compton process and bremsstrahlung using axioelectric effect, JETP Lett. 95 (2012) 379. arXiv:1206.4142.
[88] A. Ljubicic, D. Kekez, Z. Krecak, T. Ljubicic, Search for hadronic axions using axioelectric effect, Phys.Lett. B599 (2004) 143–147. arXiv:hep-ex/0403045, doi:10.1016/j.physletb.2004.08.038.
[89] S. J. Asztalos, et al., A SQUID-based microwave cavity search for dark-matter axions, Phys. Rev. Lett. 104 (2010) 041301. arXiv:0910.5914, doi:10.1103/PhysRevLett.104.041301.
[90] K. Zioutas, et al., First results from the CERN Axion Solar Telescope (CAST), Phys. Rev. Lett.94 (2005) 121301. arXiv:hep-ex/0411033, doi:10.1103/PhysRevLett.94.121301.
[91] J. Redondo, Solar axion flux from the axion-electron couplingarXiv:1310.0823.
[92] D. Z. Freedman, Coherent neutrino nucleus scattering as a probe of the weak neutral current, Phys. Rev. D9 (1974) 1389–1392. doi:10.1103/PhysRevD.9.1389.
[93] D. Akimov, et al., Observation of Coherent Elastic Neutrino-Nucleus ScatteringarXiv:1708.01294, doi:10.1126/science.aao0990.
[94] A. Drukier, L. Stodolsky, Principles and Applications of a Neutral Current Detector for Neutrino Physics and Astronomy, Phys. Rev. D30 (1984) 2295, [,395(1984)]. doi:10.1103/PhysRevD.30.2295.
[95] J. Monroe, the Dm-Tpc Collaboration, Neutrino backgrounds to dark matter searches and directionality, Journal of Physics: Conference Series 136 (2) (2008) 022037.
URL http://stacks.iop.org/1742-6596/136/i=2/a=022037
[96] A. J. Anderson, J. M. Conrad, E. Figueroa-Feliciano, K. Scholberg, J. Spitz, Coherent Neutrino Scattering in Dark Matter Detectors, Phys. Rev. D84 (2011) 013008. arXiv:1103.4894, doi:10.1103/PhysRevD.84.013008.
[97] W. C. Haxton, R. G. Hamish Robertson, A. M. Serenelli, Solar Neutrinos: Status and Prospects, Ann. Rev. Astron. Astrophys. 51 (2013) 21–61. arXiv:1208.5723, doi:10.1146/annurev-astro-081811-125539.
[98] G. Bellini, et al., Neutrinos from the primary protonâĂŞproton fusion process in the Sun, Nature 512 (7515) (2014) 383–386. doi:10.1038/nature13702.
[99] L. E. Strigari, Neutrino floor at ultralow threshold, Phys. Rev. D93 (10) (2016) 103534. arXiv:1604.00729, doi:10.1103/PhysRevD.93.103534.
[100] G. Bellini, et al., Final results of Borexino Phase-I on low energy solar neutrino spectroscopy, Phys. Rev. D89 (11) (2014) 112007. arXiv:1308.0443, doi:10.1103/PhysRevD.89.112007.
[101] N. Grevesse, A. J. Sauval, Standard Solar Composition, Space Sci. Rev. 85 (1998) 161–174. doi:10.1023/A:1005161325181.
[102] F. L. Villante, A. M. Serenelli, F. Delahaye, M. H. Pinsonneault, The chemical composition of the Sun from helioseismic and solar neutrino data, Astrophys. J. 787 (2014) 13. arXiv:1312.3885, doi:10.1088/0004-637X/787/1/13.
[103] N. Vinyoles, A. M. Serenelli, F. L. Villante, S. Basu, J. BergstrÃűm, M. C. Gonzalez-Garcia, M. Maltoni, C. PeÃśa-Garay, N. Song, A new Generation of Standard Solar Models, Astrophys. J. 835 (2) (2017) 202. arXiv:1611.09867, doi:10.3847/1538-4357/835/2/202.
[104] J. Billard, L. E. Strigari, E. Figueroa-Feliciano, Solar neutrino physics with low-threshold dark matter detectors, Phys. Rev. D91 (9) (2015) 095023. arXiv:1409.0050, doi:10.1103/PhysRevD.91.095023.
[105] D. G. CerdeÃśo, M. Fairbairn, T. Jubb, P. A. N. Machado, A. C. Vincent, C. BÅŞhm, Physics from solar neutrinos in dark matter direct detection experiments, JHEP 05 (2016) 118, [Erratum: JHEP09,048(2016)]. arXiv:1604.01025, doi:10.1007/JHEP09(2016)048,10.1007/JHEP05(2016)118.
[106] K. Scholberg, Supernova Neutrino Detection, Ann. Rev. Nucl. Part. Sci. 62 (2012) 81–103. arXiv:1205.6003, doi:10.1146/annurev-nucl-102711-095006.
[107] J. Barranco, A. Bernal, D. Delepine, Diffuse neutrino supernova background as a cosmological testarXiv:1706.03834.
[108] R. F. Lang, C. McCabe, S. Reichard, M. Selvi, I. Tamborra, Supernova neutrino physics with xenon dark matter detectors: A timely perspective, Phys.

Rev. D94 (10) (2016) 103009. arXiv:1606.09243, doi:10.1103/PhysRevD.94.103009.

[109] M. Leyton, S. Dye, J. Monroe, Exploring the hidden interior of the Earth with directional neutrino measurements, Nature Communications 8. doi:10.1038/ncomms15989.

[110] E. Bertuzzo, F. F. Deppisch, S. Kulkarni, Y. F. Perez Gonzalez, R. Zukanovich Funchal, Dark Matter and Exotic Neutrino Interactions in Direct Detection Searches, JHEP 04 (2017) 073. arXiv:1701.07443, doi:10.1007/JHEP04(2017)073.

[111] J. B. R. Battat, et al., Readout technologies for directional WIMP Dark Matter detection, Phys. Rept. 662 (2016) 1–46. arXiv:1610.02396, doi:10.1016/j.physrep.2016.10.001.

[112] A. Aleksandrov, et al., NEWS: Nuclear Emulsions for WIMP SearcharXiv:1604.04199.

[113] A. Drukier, K. Freese, A. Lopez, D. Spergel, C. Cantor, G. Church, T. Sano, New Dark Matter Detectors using DNA or RNA for Nanometer TrackingarXiv:1206.6809.

[114] Y. Hochberg, Y. Kahn, M. Lisanti, C. G. Tully, K. M. Zurek, Directional Detection of Dark Matter with 2D TargetsarXiv:1606.08849.

[115] S. Betts, et al., Development of a Relic Neutrino Detection Experiment at PTOLEMY: Princeton Tritium Observatory for Light, Early-Universe, Massive-Neutrino Yield, in: Proceedings, 2013 Community Summer Study on the Future of U.S. Particle Physics: Snowmass on the Mississippi (CSS2013): Minneapolis, MN, USA, July 29-August 6, 2013, 2013. arXiv:1307.4738.
URL http://www.slac.stanford.edu/econf/C1307292/docs/submittedArxivFiles/1307.4738.pdf

[116] P. H. Heckmann, H. Hansen, A. Flammersfeld, Die Richtungsabhängigkeit der Szintillations-Lichtausbeute von dünnen Anthrazen- und Stilben-Kristallen beim Beschuß mit α-Strahlen, Zeitschrift fur Physik 162 (1961) 84–92. doi:10.1007/BF01342470.

[117] P. Belli, R. Bernabei, C. Bacci, A. Incicchitti, D. Prosperi, Identifying a 'dark matter' signal by nonisotropic scintillation detector, Nuovo Cim.C15 (1992) 475–479.

[118] N. J. C. Spooner, J. W. Roberts, D. R. Tovey, Measurements of carbon recoil scintillation efficiency and anisotropy in stilbene for WIMP searches with direction sensitivity, in: Proceedings, 1st International Workshop on The identification of dark matter (IDM 1996), 1996, pp. 481–486.

[119] Y. Shimizu, M. Minowa, H. Sekiya, Y. Inoue, Directional scintillation detector for the detection of the wind of WIMPs, Nucl. Instrum. MethodsA496 (2003) 347–352. arXiv:astro-ph/0207529, doi:10.1016/S0168-9002(02)01661-3.

[120] F. Cappella, et al., On the potentiality of the $ZnWO_4$ anisotropic detectors to measure the directionality of Dark Matter, Eur. Phys. J. C73 (1) (2013) 2276. doi:10.1140/epjc/s10052-013-2276-2.

[121] H. Sekiya, M. Minowa, Y. Shimizu, Y. Inoue, W. Suganuma, Measurements of anisotropic scintillation efficiency for carbon recoils in a stilbene crystal for dark matter detection, Phys. Lett. B571 (2003) 132–138. arXiv:astro-ph/0307384, doi:10.1016/j.physletb.2003.07.077.

[122] D. Nygren, Columnar recombination: a tool for nuclear recoil directional sensitivity in a xenon-based direct detection WIMP search, J.Phys.Conf.Ser. 460 (2013) 012006. doi:10.1088/1742-6596/460/1/012006.

[123] G. Jaffé, Zur theorie der ionisation in kolonnen, Annalen der Physik 347 (12) (1913) 303–344.

[124] Y. Nakajima, A. Goldschmidt, M. Long, D. Nygren, C. Oliveira, J. Renner, Micro-physics simulations of columnar recombination along nuclear recoil tracks in high-pressure Xe gas for directional dark matter searches, J. Phys. Conf. Ser. 650 (2015) 012003. arXiv:1505.03586, doi:10.1088/1742-6596/650/1/012003.

[125] Y. Nakajima, A. Goldshmidt, H. S. Matis, T. Miller, D. R. Nygren, C. A. B. Oliveira, J. Renner, Measurement of scintillation and ionization yield with high-pressure gaseous mixtures of Xe and TMA for improved neutrinoless double beta decay and dark matter searches, JINST 11 (03) (2016) C03041. arXiv:1511.02257, doi:10.1088/1748-0221/11/03/C03041.

[126] L. M. Capparelli, G. Cavoto, D. Mazzilli, A. D. Polosa, Directional Dark Matter Searches with Carbon Nanotubes, Phys. Dark Univ.9-10 (2015) 24–30, [Erratum: Phys. Dark Univ.11,79(2016)]. arXiv:1412.8213, doi:10.1016/j.dark.2015.12.004,10.1016/j.dark.2015.08.002.

[127] J. F. Ziegler, P. Biersack, The Stopping and Range of Ions in Matter, Pergamon Press, New York, 1985.

[128] S. Biagi, Magoltz web page at CERNdoi:http://magboltz.web.cern.ch/magboltz/.